Atmos. Chem. Phys., 9, 5877–5903, 2009
www.atmos-chem-phys.net/9/5877/2009/

Atmospheric Chemistry and Physics

Inverse modeling and mapping US air quality influences of inorganic $PM_{2.5}$ precursor emissions using the adjoint of GEOS-Chem

D. K. Henze[1,3,*], **J. H. Seinfeld**[2], **and D. T. Shindell**[3]

[1]Earth Institute, Columbia University, New York, NY, USA
[2]Division of Chemistry and Chemical Engineering, California Institute of Technology, Pasadena, CA, USA
[3]NASA Goddard Institute for Space Studies, New York, NY, USA
[*]now at: Department of Mechanical Engineering, University of Colorado, Boulder, CO, USA

Received: 1 July 2008 – Published in Atmos. Chem. Phys. Discuss.: 8 August 2008
Revised: 10 August 2009 – Accepted: 10 August 2009 – Published: 19 August 2009

Abstract. Influences of specific sources of inorganic $PM_{2.5}$ on peak and ambient aerosol concentrations in the US are evaluated using a combination of inverse modeling and sensitivity analysis. First, sulfate and nitrate aerosol measurements from the IMPROVE network are assimilated using the four-dimensional variational (4D-Var) method into the GEOS-Chem chemical transport model in order to constrain emissions estimates in four separate month-long inversions (one per season). Of the precursor emissions, these observations primarily constrain ammonia (NH_3). While the net result is a decrease in estimated US NH_3 emissions relative to the original inventory, there is considerable variability in adjustments made to NH_3 emissions in different locations, seasons and source sectors, such as focused decreases in the midwest during July, broad decreases throughout the US in January, increases in eastern coastal areas in April, and an effective redistribution of emissions from natural to anthropogenic sources. Implementing these constrained emissions, the adjoint model is applied to quantify the influences of emissions on representative $PM_{2.5}$ air quality metrics within the US. The resulting sensitivity maps display a wide range of spatial, sectoral and seasonal variability in the susceptibility of the air quality metrics to absolute emissions changes and the effectiveness of incremental emissions controls of specific source sectors. NH_3 emissions near sources of sulfur oxides (SO_x) are estimated to most influence peak inorganic $PM_{2.5}$ levels in the East; thus, the most effective controls of NH_3 emissions are often disjoint from locations of peak NH_3 emissions. Controls of emissions from industrial sectors of SO_x and NO_x are estimated to be more effective than surface emissions, and changes to NH_3 emissions in regions dominated by natural sources are disproportionately more effective than regions dominated by anthropogenic sources. NO_x controls are most effective in northern states in October; in January, SO_x controls may be counterproductive. When considering ambient inorganic $PM_{2.5}$ concentrations, intercontinental influences are small, though transboundary influences within North America are significant, with SO_x emissions from surface sources in Mexico contributing almost a fourth of the total influence from this sector.

Correspondence to: D. K. Henze
(daven.henze@colorado.edu)

1 Introduction

The persistence of airborne fine particulate matter in heavily populated areas poses a significant health hazard (Pope, 2000; Pope et al., 2002). In the United States, it is estimated that 90 million people live in areas where yearly average mass concentrations of particles with an aerodynamic diameter less than 2.5 μm ($PM_{2.5}$) exceed the National Ambient Air Quality Standards (NAAQS) (EPA, 2002, 2004). On average, about half of the mass of such aerosol is composed of the inorganic species sulfate (SO_4^{2-}), nitrate (NO_3^-) and ammonium (NH_4^+), which will be the focus of the present work. Formation of effective regulatory measures for control of inorganic $PM_{2.5}$ requires both comprehensive estimates of existing inorganic aerosol distributions and also a means of assessing how emissions abatement would alter such distributions. Both of these tasks are made difficult by the fact that inorganic $PM_{2.5}$ is generally not directly emitted; rather, it is formed secondarily in the atmosphere via chemical and thermodynamic transformations of gas-phase precursors that may potentially emanate far from nonattainment regions.

Published by Copernicus Publications on behalf of the European Geosciences Union.

Existing studies of sources of secondary inorganic aerosol within the continental US follow several approaches. Detailed field measurements combined with meteorological back trajectories and process analysis provide insight into the nature of the governing chemical mechanisms and contributing sources (e.g., Quinn et al., 2006; Brock et al., 2008; de Gouw et al., 2008). Lagrangian chemical trajectory models are used to further assess the role of various physical and chemical processes along specific source – receptor paths (Yu et al., 2008). Factor analysis of $PM_{2.5}$ concentrations is used to statistically estimate contributions from emissions source sectors to a set of measurements (Brinkman et al., 2006; Lee et al., 2008), typically on the scale of individual metropolitan areas. Eulerian chemical transport models can reveal the influence of sources of inorganic $PM_{2.5}$ by comparing model simulations with and without emissions (toggling) from specific sectors or locations, such as transboundary vs. local emissions (Park et al., 2004; Knipping et al., 2006; Chin et al., 2007). Direct decoupled sensitivity analysis is a more efficient method than emissions toggling for estimating the sensitivity of aerosol concentrations over the entire model domain with respect to a large number of sources without perturbing the forward model state (Napelenok et al., 2006). More directly, tracking sources of inorganic $PM_{2.5}$ using emissions-labeled tracers is used to explicitly apportion aerosol estimates by source on local to hemispheric scales (Kleeman and Cass, 2001; Ying and Kleeman, 2006; Ying et al., 2007; Liu et al., 2008). Additional examples of these approaches to source analysis for secondary aerosols in studies throughout the Northern Hemisphere can be found in Benkovitz et al. (2006). Ultimately, analysis of inorganic $PM_{2.5}$ sources on a continental scale is contingent upon comprehensive knowledge of the aerosol distribution. However, observations are often incomplete in their spatial or temporal coverage, and model estimates can be subject to significant uncertainties. Hence, continued analysis of inorganic $PM_{2.5}$ sources comprises both further utilization of aerosol measurements and improvement of forward model estimates.

The approach to inorganic $PM_{2.5}$ source analysis taken in this work consists of two stages. The first stage is to constrain model estimates of aerosol precursor emissions and the resulting aerosol distributions by assimilating chemically speciated measurements of aerosol concentrations. Data assimilation techniques provide a framework for combining observations and models to form an optimal estimate of the chemical state of the atmosphere. Methods based in parameter optimization (as opposed to interpolation or nudging) can be used for inverse modeling, wherein observations are used to constrain estimates of model parameters that are both influential and uncertain (typically emissions). For inorganic $PM_{2.5}$, the key emissions of gas-phase precursors are sulfur dioxide (SO_2, often considered collectively with SO_4^{2-} emissions as SO_x), nitrogen oxides (NO_x) and ammonia (NH_3). NH_3 is recognized as being both highly uncertain and influential for aerosol formation and thus a critical factor for improving estimated distributions of nitrate aerosol in the continental US (Park et al., 2004; Yu et al., 2005; Nowak et al., 2006; Park et al., 2006; Liao et al., 2007; Zhang et al., 2008; Wu et al., 2008; Stephen and Aneja, 2008). Previous inverse modeling studies of NH_4^+ in the US using a Discrete Kalman filter (Gilliland and Abbitt, 2001) estimated improved monthly emissions scaling factors for total US NH_3 emissions using observations of ammonium wet deposition (Gilliland et al., 2003, 2006). In a separate effort, Mendoza-Dominguez and Russell (2000, 2001) optimized domain-wide emissions scaling factors for eight types of emissions (including SO_x, NO_x and NH_3) over the eastern US using observations of gas-phase inorganic and organic species and speciated fine particles. In these studies, the spatial distributions of emissions were assumed to be known; the magnitude of the emissions were adjusted using domain-wide scaling factors. For a sensitivity study in Gilliland et al. (2006), two separate scaling factors for Eastern and Western locations were considered. These studies provide valuable constraints on total emissions budgets and highlight the importance of improving estimates of inorganic $PM_{2.5}$ precursor emissions.

The present works seeks to improve upon previous inverse modeling studies via application of the four-dimensional variational data assimilation technique (4D-Var) (Kalnay, 2003) using the adjoint of the GEOS-Chem chemical transport model (Henze et al., 2007). The adjoint of the GEOS-Chem model was developed specifically for inverse modeling of $PM_{2.5}$ observations with explicit inclusion of gas-phase chemistry, heterogeneous chemistry, and treatment of the thermodynamic couplings of the sulfate – ammonium – nitrate – water aerosol system; it is thus uniquely capable of exploiting aerosol-phase measurements in novel ways. The adjoint model is used to calculate gradients of the error weighted squared difference between model predictions and observations with respect to emissions. An adjoint model is an efficient means of calculating the sensitivities of this type of model response with respect to numerous ($\mathcal{O}(10^6)$) model parameters simultaneously, affording optimization of parameters on a resolution commensurate with that of the forward model itself. This allows refinement of both the overall magnitude and the spatial distributions of emissions, distinguishing between different emission source sectors, and quantification of the influence of other uncertain model parameters such as initial conditions and heterogeneous uptake coefficients. The feedbacks between the inorganic $PM_{2.5}$ species and their gas-phase precursors have been noted as a hindrance to inverse modeling estimates of NH_3 emissions using aerosol NH_4^+ measurements (Pinder et al., 2006); here these feedbacks are exploited by using surface measurements of sulfate and nitrate aerosol concentrations to constrain estimates of precursor emissions, particularly NH_3.

In addition to its utility in inverse modeling, an adjoint model itself is a novel tool for evaluating sources pertinent

to air quality regulations (Hakami et al., 2006). In the second stage of this work (Sect. 5), the adjoint of GEOS-Chem is used to generate maps of the influence of inorganic $PM_{2.5}$ precursor emissions on representative air quality attainment metrics. Emissions from various sectors and locations are then ranked according to their influence on nonattainment. These results are contingent upon the best estimate of the precursor emissions themselves, and are thus presented following introduction of the forward model (Sect. 2), description of the adjoint method for calculating discrete model sensitivities (Sect. 3), and results of the inverse modeling (Sect. 4). While adjoint sensitivity analysis is not strictly a method for source apportionment, it does have several attractive aspects for estimating the incremental influence of specific sources on air quality attainment. Unlike analysis of meteorological back trajectories or statistical factor analysis, this approach accounts for chemical and physical processing and transport combined. The influence of emissions are readily obtained for each location and for all types at a computational expense of no more than three times that of a normal forward model simulation. This is an advantage over emissions-labeling, Lagrangian modeling or emissions toggling, each of which increases in computational expense as the number of source regions/types/times is refined. Finally, the analysis can be performed around the current model state, providing estimates of the immediate consequences of emissions changes, in contrast to estimates that rely in part on non-physical emissions-free simulations, potentially triggering nonlinear model responses (Liu et al., 2008).

2 Forward model description

The GEOS-Chem chemical transport model is used to estimate ambient concentrations of inorganic aerosol over the US for the months of January 2001, through January 2002. The model is driven using assimilated meteorology from the Goddard Earth Observing System (GEOS-3) of the NASA Global Modeling and Assimilation Office (GMAO). GEOS-3 data sets are down-sampled to a resolution of $4^\circ \times 5^\circ$ to facilitate detailed simulation of tropospheric gas-phase chemistry, discussed fully in works such as Bey et al. (2001), Li et al. (2001) and Martin et al. (2002). The present study uses model version 6-02-05, which includes an online secondary inorganic aerosol simulation introduced and described in detail by Park et al. (2004). Model estimates of inorganic $PM_{2.5}$ have been compared to surface measurements (Park et al., 2004, 2006; Liao et al., 2007) and measurements from aircraft campaigns (Heald et al., 2005, 2006b); here we reiterate key features of the inorganic aerosol simulation.

Fine mode (aerodynamic diameter less than $2.5\,\mu$m) inorganic aerosol is calculated as the mass of aerosol-phase SO_4^{2-}, NH_4^+ and NO_3^- that forms from the gas-phase precursors sulfuric acid (H_2SO_4), NH_3, and nitric acid (HNO_3). H_2SO_4 is formed from oxidation of SO_2 by OH in the gas-phase, and, more importantly, by H_2O_2 and O_3 in clouds. As H_2SO_4 readily partitions into the particle phase, it is always treated as aerosol sulfate. Thermodynamic equilibrium of aerosol NH_4^+ and NO_3^- with their gas-phase counterparts (NH_3 and HNO_3) is calculated using the MARS-A routine of Binkowski and Roselle (2003), which allows for formation of $(NH_4)_2SO_4$ and, if excess NH_3 is available, NH_4NO_3, though formation of aerosol NO_3^- can be enhanced by cold or moist conditions. Additional couplings between gas and aerosol phases treated in the model include formation of HNO_3 through heterogeneous reaction of N_2O_5 with water, where the reaction probability is calculated as a function of aerosol type, available surface area, temperature, and relative humidity (Evans and Jacob, 2005). Uptake of NO_2 and NO_3 on aerosol surfaces is described in Martin et al. (2003). The formation of H_2O_2 from heterogenous uptake of HO_2 (Thornton and Abbatt, 2005) is also considered.

Anthropogenic emissions of NO_x and SO_x are taken from the Global Emission Inventory Activity (GEIA) database for the year 1985 (Benkovitz et al., 1996), scaled according to fossil fuel usage for the year 1998 (Bey et al., 2001). NH_3 emissions from anthropogenic sources (domesticated animals, fertilizers, human bodies, industry, fossil fuels) and natural sources (oceans, crops, soils, wild animals) are based on data from the 1990 GEIA inventory of Bouwman et al. (1997), with additional contributions owing to biomass burning and biofuel use from inventories by Duncan et al. (2003) and Yevich and Logan (2003). The total yearly source of NH_3 in the United States is scaled to match that of Gilliland et al. (2003), while monthly variability is calculated according to an exponential temperature scaling (Adams et al., 1999). Dry deposition of all types of aerosol is calculated using a resistance-in-series model (Wesely, 1989; Wang et al., 1998); wet removal is described in Jacob et al. (2000).

3 Adjoint modeling

Founded in optimal control theory and variational calculus, adjoint methods were initially suggested as approaches to source analysis of atmospheric tracers several decades ago (Lions, 1971; Marchuk, 1974). By the late 1990s, the method was applied to chemical transport models of the stratosphere (Fisher and Lary, 1995) and troposphere (Elbern et al., 1997). The method was used to constrain emissions in an Eulerian air quality model of chemically active species in the troposphere by Elbern et al. (2000). Subsequent investigations of emissions have been explored with adjoints of chemical transport models such as CHIMERE (Vautard et al., 2000; Menut, 2003; Schmidt and Martin, 2003), Polair (Quelo et al., 2005), the CIT model (Martien et al., 2006; Martien and Harley, 2006), STEM (Sandu et al., 2005a; Hakami et al., 2005), DRAIS (Nester and Panitz, 2006), CMAQ (Hakami et al., 2007), IMAGES (Müller and

Stavrakou, 2005; Stavrakou and Muller, 2006; Stavrakou et al., 2008), and GOCART (Dubovik et al., 2004, 2008).

While previous chemical transport adjoint models have focused largely on gas-phase processes and observations, the focus of the present work is on aerosols. Henze et al. (2004) and Sandu et al. (2005b) used the adjoint method for inverse modeling of aerosol distributions in box model simulations. Hakami et al. (2005) used the adjoint of STEM for inverse modeling of black carbon aerosol, treated as an inert tracer. The inverse modeling of Dubovik et al. (2008) focused on constraining global estimates of SO_x and primary aerosol emissions with MODIS observations using the adjoint of the GOCART model; GOCART considers secondary formation of sulfate from SO_2 using prescribed oxidant fields, as well as carbonaceous, dust and sea salt aerosol (Chin et al., 2000).

The GEOS-Chem aerosol simulation is based on the GOCART model, particularly for wet scavenging, with updates described by Park et al. (2004). GEOS-Chem and its adjoint also includes ammonium and nitrate aerosol, the thermodynamics of the sufate-ammonium-nitrate-water aerosol system, and detailed tropospheric gas-phase chemistry for online calculation of oxidation of aerosol precursors. A full description of the GEOS-Chem adjoint model is given in Henze et al. (2007), where the adjoint of each individual physical and chemical model operator is derived and validated, and pseudo-observations are used to assess the potential inverse modeling performance. Subsequently, the GEOS-Chem adjoint model has been updated to include online calculations of the heterogenous reaction rates (and the corresponding adjoint), and sensitivities with respect to emissions of NO_x from soil and lightning. The GEOS-Chem adjoint has also been further developed for inverse modeling CO emissions using remote sensing observations (Kopacz et al., 2009). In the remainder of this section, the general approach to adjoint sensitivity analysis is reviewed.

A chemical transport model can be viewed as a numerical operator, F, acting on a vector of initial concentrations, $\boldsymbol{c}^0$, and a vector of parameters, $\boldsymbol{p}$, to yield an estimate of the evolved concentrations at a later time, N,

$$\boldsymbol{c}^N = F(\boldsymbol{c}^0, \boldsymbol{p}), \tag{1}$$

where $\boldsymbol{c}$ is the vector of all K tracer concentrations, $\boldsymbol{c}^n = [c_1^n, \ldots, c_k^n, \ldots, c_K^n]^T$ at time step n. In practice, F comprises many individual operators representing various physical processes. For the moment, let F^n represent a portion of the discrete forward model that advances the concentration vector from time step n to step $n+1$.

$$\boldsymbol{c}^{n+1} = F^n(\boldsymbol{c}^n, \boldsymbol{p}), \tag{2}$$

The adjoint model is used to calculate the sensitivity of a scalar model response function, $\mathcal{J}$, with respect to the model parameters, $\boldsymbol{p}$. The response function may depend only upon a temporal subset of concentrations, Ω_n, or a subset of chemical species or locations, $\hat{c}_k^n, k \in \Omega_k$, and may include a term explicitly depending upon the parameters, $J_p(\boldsymbol{p})$,

$$\mathcal{J} = \sum_{n \in \Omega_n} J^n(\hat{\boldsymbol{c}}^n) + J_p(\boldsymbol{p}). \tag{3}$$

Assuming the parameters are constant, $J_p(\boldsymbol{p})$ does not have a time step index. In practice the definitions of Ω, J^n and J_p are very application-specific. For the following derivation it is simply assumed that the response domain includes all species at all times such that

$$\mathcal{J} = \sum_{n=0}^{N} J^n(\boldsymbol{c}^n) + J_p(\boldsymbol{p}). \tag{4}$$

The purpose of the adjoint model is to calculate the sensitivity of the response with respect to the model parameters. As will become evident, it is first necessary to calculate the sensitivity of the model response with respect to species concentrations at every time step n in the model,

$$\nabla_{\boldsymbol{c}^n}\mathcal{J} = \left(\frac{\partial \mathcal{J}}{\partial \boldsymbol{c}^n}\right)^T = \sum_{n'=n}^{N} \left(\frac{\partial J^{n'}}{\partial \boldsymbol{c}^n}\right)^T \tag{5}$$

$$\left(\text{note: } \frac{\partial J^{n'}}{\partial \boldsymbol{c}^n} = 0 \text{ for } n' < n\right).$$

The Jacobian matrix of the model operator around any given time step can be written as

$$\frac{\partial \boldsymbol{c}^{n+1}}{\partial \boldsymbol{c}^n} = \frac{\partial F^n(\boldsymbol{c}^n)}{\partial \boldsymbol{c}^n} \equiv \mathbf{F}_c^n \tag{6}$$

and similarly,

$$\frac{\partial \boldsymbol{c}^{n+1}}{\partial \boldsymbol{p}} = \frac{\partial F^n(\boldsymbol{c}^n)}{\partial \boldsymbol{p}} \equiv \mathbf{F}_p^n. \tag{7}$$

Using the chain rule, the sum on the right hand side of Eq. (5) is expanded,

$$\begin{aligned}\nabla_{\boldsymbol{c}^n}\mathcal{J} = {} & (\mathbf{F}_c^n)^T(\mathbf{F}_c^{n+1})^T \cdots (\mathbf{F}_c^{N-1})^T \left(\frac{\partial J^N}{\partial \boldsymbol{c}^N}\right)^T \\ & + (\mathbf{F}_c^n)^T(\mathbf{F}_c^{n+1})^T \cdots (\mathbf{F}_c^{N-2})^T \left(\frac{\partial J^{N-1}}{\partial \boldsymbol{c}^{N-1}}\right)^T + \cdots \\ & + \left(\frac{\partial J^n}{\partial \boldsymbol{c}^n}\right)^T.\end{aligned} \tag{8}$$

The sensitivity of the response with respect to the model parameters (assumed here not to depend on the time step n) can then be written as

$$\begin{aligned}\nabla_{\boldsymbol{p}}\mathcal{J} = {} & (\mathbf{F}_p^{N-1})^T \nabla_{\boldsymbol{c}^N}\mathcal{J} \\ & + (\mathbf{F}_p^{N-2})^T \nabla_{\boldsymbol{c}^{N-1}}\mathcal{J} + \ldots \\ & + (\mathbf{F}_p^0)^T \nabla_{\boldsymbol{c}^1}\mathcal{J} + \left(\frac{\partial J_p}{\partial \boldsymbol{p}}\right)^T.\end{aligned} \tag{9}$$

In this context, the adjoint method is essentially just an approach to evaluating Eqs. (8) and (9) that is computationally efficient when $\dim\{\boldsymbol{c}\}$ and $\dim\{\boldsymbol{p}\}>\dim\{\mathcal{J}\}$ (Giering and Kaminski, 1998). The adjoint sensitivity variables are defined as $\boldsymbol{\lambda}_c^n=\nabla_{\boldsymbol{c}^n}\mathcal{J}$ and $\boldsymbol{\lambda}_p=\nabla_{\boldsymbol{p}}\mathcal{J}$, where the subscripts c and p indicate sensitivity with respect to $\boldsymbol{c}$ and $\boldsymbol{p}$, respectively. Initializing

$$\boldsymbol{\lambda}_c^N=\left(\frac{\partial J^N}{\partial \boldsymbol{c}^N}\right)^T \text{ and } \boldsymbol{\lambda}_p=\left(\frac{\partial J_p}{\partial \boldsymbol{p}}\right)^T,$$

adjoint sensitivities are found by evaluating the following update formulas iteratively from $n=N,\ldots,1$,

$$\boldsymbol{\lambda}_c^{n-1}=(\mathbf{F}_c^{n-1})^T\boldsymbol{\lambda}_c^n+\left(\frac{\partial J^{n-1}}{\partial \boldsymbol{c}^{n-1}}\right)^T, \quad (10)$$

$$\boldsymbol{\lambda}_p=(\mathbf{F}_p^{n-1})^T\boldsymbol{\lambda}_c^n+\boldsymbol{\lambda}_p, \quad (11)$$

The $\frac{\partial J^n}{\partial \boldsymbol{c}^n}$ terms are referred to as the adjoint forcings as their role in the adjoint model is analogous to that of emissions in the forward model (for further details, see the continuous forward and adjoint model equations in Sandu et al., 2005a). While calculation of adjoint values using this algorithm is straightforward, there are a few subtleties worth mentioning. First, evaluating sensitivities with respect to model parameters requires having first calculated sensitivities with respect to concentrations. Since evaluation of Eq. (8) is much more computationally expensive than evaluation of Eq. (9), the overall computational cost is largely invariant to the number of parameters considered. Second, while solving Eq. (11) iteratively along with Eq. (10) is not necessary, it is computationally preferable as values of $\boldsymbol{\lambda}_c^n$ and $\mathbf{F}_p^n$ need not be stored for more than a single step.

4 Inverse modeling

4.1 Cost function

Inverse modeling is the process by which measurements are used to reduce the set of possible models from all that are consistent with prior information to a reduced set (the inverse model solution) by rejecting those that do not likely represent the observations (Tarantola, 2006). A range of models is typically constructed using control parameters,

$$\boldsymbol{\sigma}=[\sigma_1,\sigma_2,\ldots,\sigma_M]^T,$$

which are used to adjust elements of the vector of model parameters, $\boldsymbol{p}$, via application as scaling factors[1],

$$p=p_a e^{\sigma},$$

[1]The use of scaling factors to adjust the model parameters is advantageous as it gives equal weight to all parameters, regardless of magnitude or unit. The use of log-normal scaling factors ($\sigma=ln(p/p_a)$) has several benefits over linear scaling ($\sigma=p/p_a$) for the current application (Tarantola, 2005). Increasing or decreasing order of magnitude changes to p are reflected as changes to the absolute value of σ and are thus penalized equally in the cost function, values of p are implicitly not allowed to change sign, and the uncertainty of the scaling factors can be represented as a normal distribution about 0 (for p that are strictly positive, the normal distribution of $\sigma=p/p_a$ about 1 is nonphysical as it allows a nonzero probability that $p<0$).

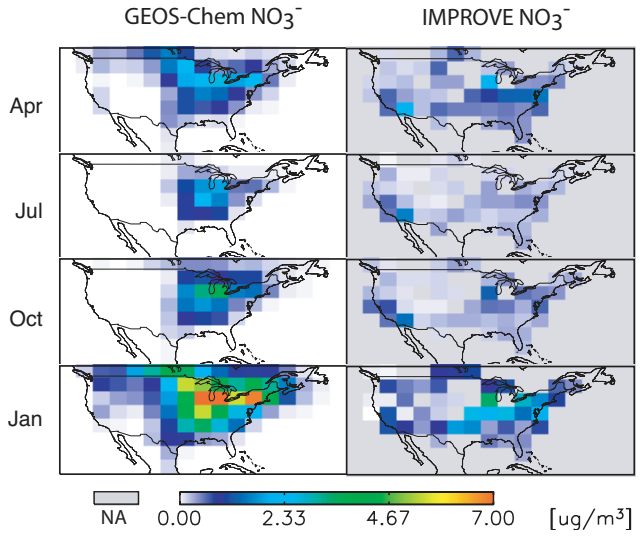

Fig. 1. Predicted (GEOS-Chem) and observed (IMPROVE) monthly average surface NO_3^-.

where $\boldsymbol{p}_a$ is the prior parameter estimate.

The inverse problem seeks $\boldsymbol{\sigma}$ that minimizes the cost function, $\mathcal{J}$, given by

$$\mathcal{J}=\frac{1}{2}\sum_{\boldsymbol{c}\in\Omega}(H\boldsymbol{c}-\boldsymbol{c}_{\text{obs}})^T\mathbf{S}_{\text{obs}}^{-1}(H\boldsymbol{c}-\boldsymbol{c}_{\text{obs}}) + \frac{1}{2}\gamma_r(\boldsymbol{\sigma}-\boldsymbol{\sigma}_a)^T\mathbf{S}_a^{-1}(\boldsymbol{\sigma}-\boldsymbol{\sigma}_a), \quad (12)$$

where $\boldsymbol{c}$ is the vector of species concentrations mapped to the observation space by H, $\boldsymbol{c}_{\text{obs}}$ is the vector of species observations, $\mathbf{S}_{\text{obs}}$ is the observation error covariance matrix, $\boldsymbol{\sigma}_a$ is the prior estimate of the parameter scaling factors (equal to 0), $\mathbf{S}_a$ is the error covariance estimate of the parameter scaling factors, γ_r is a regularization parameter, and Ω is the domain (in time, space, and chemical species) over which observations and model predictions are available. Overall, the cost function is a specific model response, the minimum value of which balances the objectives of improving model performance while ensuring the model itself remains within a reasonable range (as dictated by $\mathbf{S}_a^{-1}$) of the initial model.

4.2 Observations

Model predictions of sulfate and nitrate aerosol are compared to observations from the Interagency Monitoring of

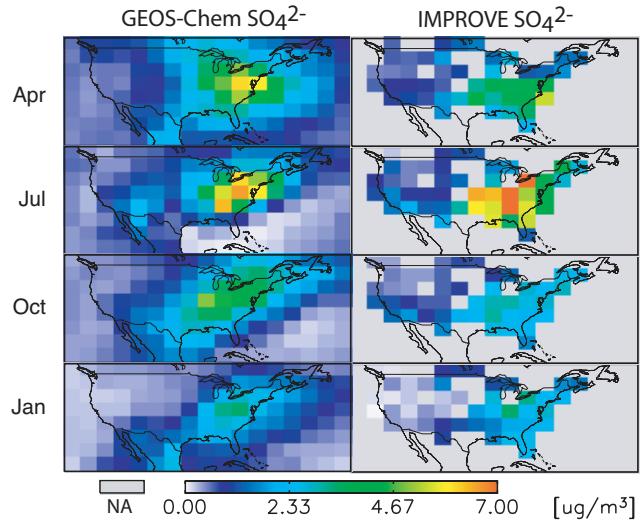

Fig. 2. Predicted (GEOS-Chem) and observed (IMPROVE) monthly average surface SO_4^{2-}.

Protected Visual Environments (IMPROVE) network (Malm et al., 1994) during the months of April, July and October 2001, and January 2002. Mass concentrations of sulfate and nitrate are determined from analysis of fine aerosol (aerodynamic diameter less than 2.5 μm) collected on teflon and nylon filters, respectively, sampled over a 24 h period every third day. Measurements from each of the ~120 IMPROVE sites are averaged on the GEOS-Chem grid, and the resulting monthly average distributions are shown in Figs. 1 and 2. The observation error covariance matrix, $\mathbf{S}_{obs}$, includes a contribution of the reported measurement error, typically 5%–10% for sulfate and 5%–30% for nitrate. As the distribution of the observations within any given model grid cell is not uniform, a representational error is also included in $\mathbf{S}_{obs}$, here assumed to be 30%.

4.3 Model parameters

In general, the parameters of a chemical transport model include emissions, boundary conditions, initial conditions, and rate parameters for deposition and chemical reactions. For this study, the parameters initially considered are scaling factors for the emissions of SO_x, NO_x and NH_3 from the source sectors listed in Table 1. Use of a global model means there are no additional boundary conditions to consider (neglecting stratospheric – tropospheric ozone exchange). Also considered are scaling factors for the initial concentrations of each tracer (initial conditions) and for several kinetic parameters, such as the heterogeneous reaction probability for formation of HNO_3 from N_2O_5, which is an important (Dentener and Crutzen, 1993), yet still highly uncertain (e.g., Brown et al., 2006), mechanism for loss of NO_x.

After a single evaluation of the adjoint model, the resulting sensitivities indicate which parameters are the most influential in determining the cost function. Figure 3 shows the sensitivity of the cost function with respect to stack emissions of SO_x, surface emissions of NO_x, anthropogenic emissions of NH_3, and natural emissions of NH_3 for January. These sensitivities are fully normalized values, $\lambda_{p_{i,m}} = \frac{\partial \mathcal{J}}{\partial p_{i,m}} \frac{p_{i,m}}{\mathcal{J}}$, shown as a percent response of $\mathcal{J}$ to fractional changes in emissions of source m in location i. These, in addition to surface emissions of SO_x and stack emissions of NO_x, have the largest sensitivities of all the emissions sectors considered in each of the months. Sensitivities of the discrepancy between observed and modeled aerosol concentrations with respect to sources of aerosol precursors outside North America are shown in the top row of Fig. 4 for April, when transport of pollution across the Pacific Ocean is most common (Yienger et al., 2000). The largest influences are from stack emissions of SO_x and surface emissions of NO_x, though with maximum sensitivities of less than 1% these sensitivities are generally several orders of magnitude smaller than those from within North America. Note that the sensitivity of the concentrations themselves (instead of $\mathcal{J}$) with respect to distant emissions can be more significant, see Sect. 5.2. The second row of Fig. 4 shows sensitivities with respect to initial conditions, displaying just the values at 933 hPa for sulfate and nitrate, which exhibit the largest influence of the initial conditions of any tracer. Values peak in the 950–750 hPa range (initial concentrations closer to the surface are less influential owing to quick depositional losses), but are still one to two orders of magnitude smaller than emissions sensitivities over the course of the simulation, as the average aerosol lifetime is much shorter than one month. Also considered are the sensitivities of the cost function with respect to rates that affect the lifetime of NO_x, and are hence critical for estimating HNO_3 and NO_3^-. For example, sensitivities with respect to heterogeneous uptake of N_2O_5 over the course of the month is found to occasionally be 35% as large as the sensitivity with respect to NO_x emissions. While this is likely a critical parameter for further research in focused areas, the overall effect of NO_x emissions was generally an order of magnitude larger in the present study. In theory, all parameters could be optimized simultaneously, even those for which the uncertainty or sensitivity is relatively small. However, to simplify the optimization process, the scaling factors for initial conditions and rate parameters are not allowed to vary, as, assuming all are equally uncertain, they are found to be much less critical than emissions parameters. Overall, the set of variable model parameters comprises monthly scaling factors in each grid cell for emissions of each species listed in Table 1.

A key aspect of inverse modeling is specification of the error covariance matrix, $\mathbf{S}_a$, of the variable parameters. For the base case inversion, the emissions of anthropogenic NO_x and SO_x are assigned a standard error in each grid cell of 30% and 10%, respectively. The error for emissions from all other sectors is taken to be 100%. Additional inversions

Table 1. Emissions inventories treated as variable parameters.

Emitted species	Source sectors considered
SO_x	surface (anthropogenic), stack (anthropogenic), ships, biomass burning, biofuel
NH_3	anthropogenic, natural, biomass burning, biofuel
NO_x	surface (anthropogenic), stack (anthropogenic), lightning, soil

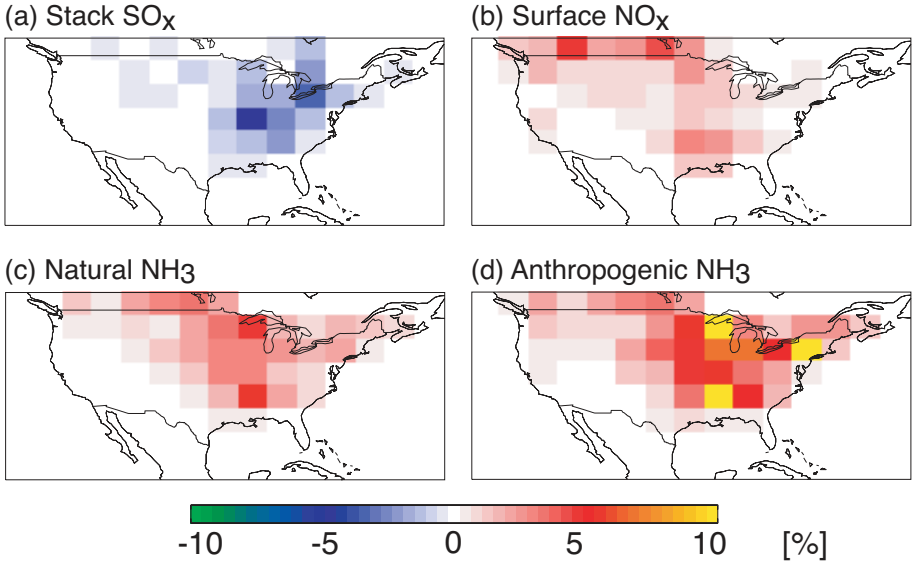

Fig. 3. Normalized sensitivities of the cost function in January with respect to emissions from: **(a)** stack SO_x, **(b)** surface NO_x, **(c)** natural NH_3, and **(d)** anthropogenic NH_3. Positive sensitivities indicate regions where a decrease in emissions would improve the overall agreement between the model and the observations ($\mathcal{J}$), and conversely for negative sensitivities.

are also performed using 50% and 100% standard error for NO_x, and 25% and 100% for SO_x; however, unless otherwise noted, results will be shown for the base case. In all cases, the errors are assumed to be uncorrelated between spatial locations and between emissions from different source sectors, hence $\mathbf{S}_a$ is diagonal. While ultimately convenient, the assumption that the errors are not correlated is in part justified in that the correlation length scale of the individual emission sources can be much less than the spatial resolution of the model (Stephen and Aneja, 2008), and partly through use of a regularization parameter to enforce a smooth solution, as discussed in the following section.

4.4 Optimization

Gradients of the cost function with respect to the parameter scaling factors calculated with the adjoint model, $\nabla_{\boldsymbol{\sigma}} \mathcal{J}$, are supplied to an optimization routine (the quasi-Newton L-BFGS-B optimization routine (Byrd et al., 1995; Zhu et al., 1994)) and the minimum of the cost function is sought iteratively. At each iteration, improved estimates of the model parameters are implemented and the forward model solution is recalculated. Figure 5 shows a typical evolution of the cost function and the gradient norm for successive function evaluations. In this case (each parameter assumed a 100% error), the cost function is reduced by 70%, and the norm of the gradient (a measure of the size of the adjoint sensitivities) is reduced by more than two orders of magnitude after 14 function evaluations, at which point the minimization is considered to have converged. Minimization of the cost function in all cases is achieved in less than 20 function evaluations.

As mentioned previously, $\mathbf{S}_a$ is assumed to be diagonal. The significance of the prior information is thus more of a smoothness constraint than a rigorous estimate of prior uncertainty (Rodgers, 2000). The regularization parameter, γ_r, is used to balance the two terms of the cost function, which can be written as:

$$\mathcal{J} = J_{\text{prediction}} + \gamma_r J_{\text{parameter}}.$$

These terms represent the total prediction error incurred for departure of model predictions from the observations, $J_{\text{prediction}}$, and the penalty error incurred for departure from the prior parameter estimates beyond the range of prior uncertainty, $J_{\text{parameter}}$. The consequence of changing γ_r on converged values of $\mathcal{J}$ is shown in Fig. 6 for several inverse modeling tests using data from January. High values of γ_r

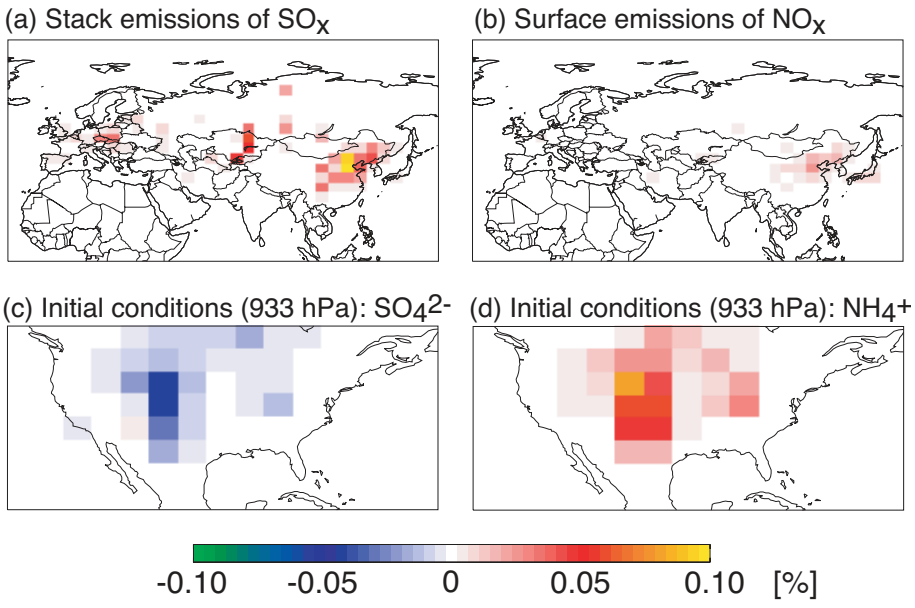

Fig. 4. Normalized sensitivities of the cost function in April with respect to **(a)** stack SO_x emissions, **(b)** NO_x surface emissions, **(c)** SO_4^{2-} initial conditions, and **(d)** NH_4^+ initial conditions. Note the scale is from −0.1% to +0.1%.

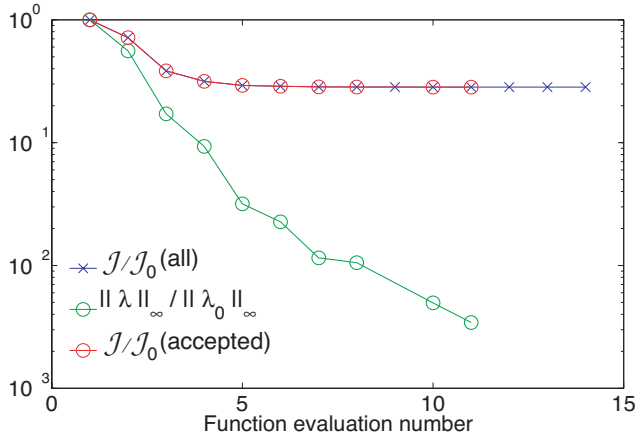

Fig. 5. Convergence of cost function (red) and gradient norm (green). The blue line shows function evaluations; open circles represent accepted iterations. Quantities are normalized with respect to their values at the initial iteration.

lead to over-smoothing of the solution with less improvement to the prediction error term, while low values of γ_r minimize the error term at the cost of greatly increasing the parameter penalty term. An optimal value can be identified at the corner near the origin of the so called L-curve (Hansen, 1998), panel (a). Another way of visualizing the balance between the two terms is shown in panel (b) of Fig. 6, where the prediction error and the penalty error are shown as a function of γ_r. In this plot the prediction error is normalized to the initial value of the cost function ($\mathcal{J}_0$=$J_{\text{prediction}}$ as $J_{\text{parameter}}$ is zero for the first iteration), while the penalty error is normalized to the value of $J_{\text{parameter}}$ when γ_r=0.01. The total error is the sum of the normalized prediction error and the normalized penalty error; the optimal value of γ_r is that which minimizes the total error. Based on combined analysis of Fig. 6a and b, the value of γ_r is taken to be 50, conservatively preferring to over-smooth the solution to the inverse problem. It is assumed that a similar range of γ_r is optimal for the remaining months, though a smaller value of γ_r=10 is used in April, July and October as $J_{\text{prediction}}$ is more than twice as large in January than in the other months.

Figure 1 shows the initial model predictions and observed monthly average aerosol nitrate, where model results are averaged over the 24 h time periods and locations for which there are observations (∼10 each month in ∼45 locations). Similar comparisons for sulfate are shown in Fig. 2. Estimates of individual 24 h sulfate concentrations over the course of the year have a mean of 1.90 μg/m^3, a root mean square (RMS) error of 1.92 μg/m^3 (n=1832), and normalized mean bias (NMB) of −0.08. The nitrate estimates have a RMS error of 1.10 μg/m^3, which is more than twice as large as the mean of 0.52 μg/m^3, and a NMB of 0.41. Previous studies comparing GEOS-Chem simulations to IMPROVE measurements have also found better agreement for sulfate than nitrate (Park et al., 2004, 2006; Liao et al., 2007). A possible source of model error is uptake of HNO_3 on mineral dust, which is a source of nitrate aerosol not considered in the model, and thus a possible model bias for locally formed aerosol in the Southwest as well as long-range transport of aerosol with dust (Malm et al., 2004; Liao et al., 2007; Fairlie et al., 2007). Formation of sulfate aerosol on sea salt is also

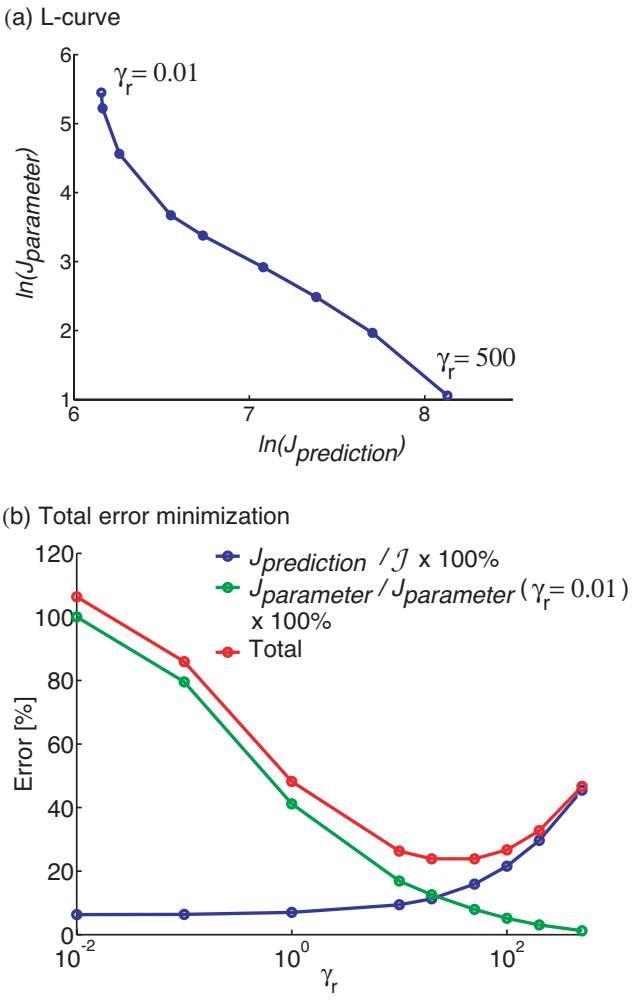

Fig. 6. The dependence of the inverse modeling solution on the regularization parameter, γ_r. Tested values are γ_r=0.01, 0.1, 1, 10, 20, 50, 100, 200, 500. **(a)** The L-curve; optimal value of γ_r=10−20. **(b)** Total error minimization: optimal value of γ_r=20−50.

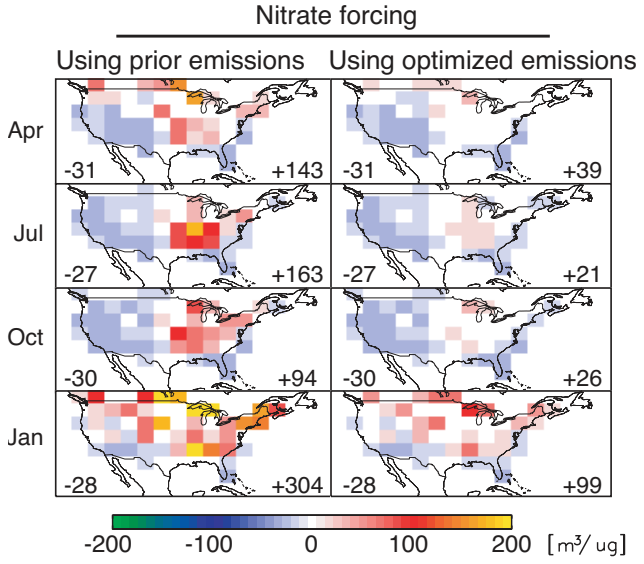

Fig. 7. Adjoint forcing of nitrate (NO_3^-) before and after optimization. Adjoint forcing is the sum of the discrepancy between modeled and observed aerosol concentrations weighted by the inverse observational error covariance. Each row corresponds to the month listed on the left. The numbers in the lower left and lower right corners of each panel give the minimum and maximum values, respectively.

not included in the model, which can impact sulfate aerosol and HNO_3 concentrations over the ocean and near coastlines (Alexander et al., 2005). However, the largest differences between the observed and modeled nitrate (in the central US) are not likely to be heavily influenced by such interactions.

Figure 7 shows the nitrate adjoint forcing in each month before and after minimization of the cost function. This adjoint forcing is a distribution of the difference between predictions and observations of aerosol nitrate weighted by the certainty in the observations, $\mathbf{S}_{\text{obs}}^{-1}$. The +/– values in the corners of each panel give the forcing range. The cost function is reduced by 30% in April and July, 40% in October, and 63% in January, The reduction in forcing shows where the nitrate simulation has improved, which is mainly in the central Midwest, the Northeast, and along the northern border. The total RMS error for nitrate over the course of the year is reduced to 0.63 μg/m^3. The sulfate aerosol forcing (not shown) is $\pm$30 μg/m^3 both before and after the optimization. The RMS error for sulfate decreases by only a few percent in April and October, by less than a percent in July, and does not change in January. That the sulfate simulation is not significantly altered is partly a consequence of the prior error specification being tighter for SO_x than for NO_x and NH_3 emissions.

Table 2 shows the change in RMS error for two additional inverse modeling solutions starting with different constraints on anthropogenic emissions of SO_x and NO_x. The looser the constraint is for these emissions, the more sulfate RMS error is improved by the inversion, while the nitrate error is relatively unaffected. However, even when all emissions constraints are equal, the decrease in the RMS error for the sulfate simulation (−8.6%) is relatively small compared to the error decrease for the nitrate simulation (−43.5%).

The representational error that contributes to $\mathbf{S}_{\text{obs}}^{-1}$ also affects the optimization. The sulfate simulation is closer to the observations on a fractional basis. Specification of the representational error in $\mathbf{S}_{\text{obs}}^{-1}$ on a fractional basis causes the sulfate prediction error to contribute less to the cost function than the nitrate prediction error, and hence the error in the sulfate simulation is not as much of a driving force for the inversion. When assumed to be a uniform fraction of the observed value throughout the model, the representational error only affects the balance between $J_{\text{prediction}}$ and $J_{\text{parameter}}$. For example, with 30% representational error and γ_r=10, the

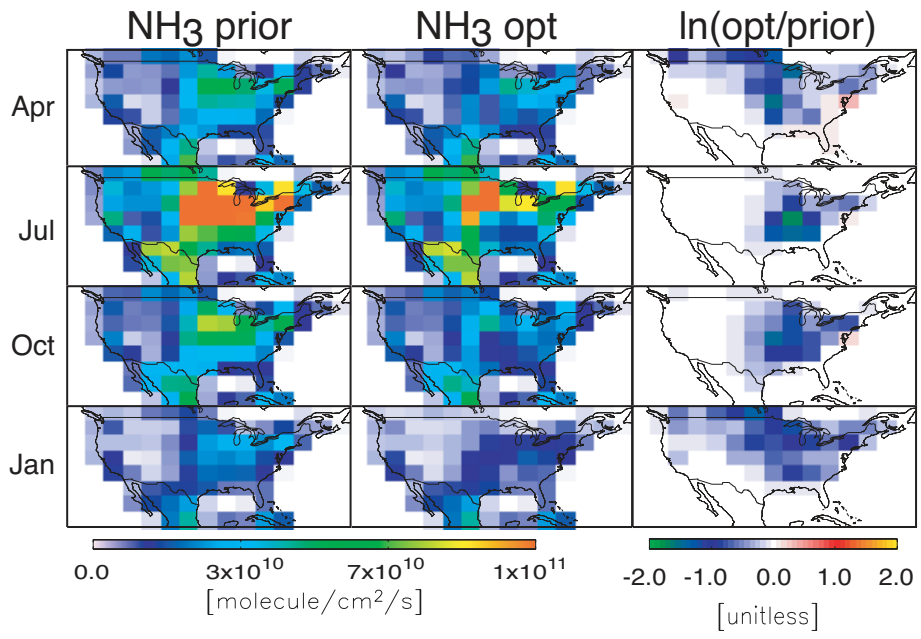

Fig. 8. Anthropogenic NH_3 emissions. The left column shows the prior inventory, the center the optimized inventory, and the right column the logarithmic scaling factors (σ).

Table 2. The effects of prior parameter error on inversion results. Changes in the total continental US emissions from all source sectors and changes in the root mean squared error (RMSE) obtained using the inverse modeling solutions obtained starting from three different sets of assumed standard errors for anthropogenic emissions of NO_x and SO_x. In each case, errors from all other source sectors have a 100% prior error. Changes ($\triangle$) are reported as (optimized-prior)/prior$\times$100%.

Initial assumed errors		Total emissions changes			Resulting error reduction	
$s_{a,NO_x,anth}$	$s_{a,SO_x,anth}$	$\triangle NH_3$	$\triangle NO_x$	$\triangle SO_x$	$\triangle$RMSE NO_3^-	$\triangle$RMSE SO_4^{2-}
30%	10%	−25.3%	−1.4%	−2.5%	−42.7%	−1.1%
50%	25%	−25.8%	−2.1%	−7.9%	−43.0%	−3.6%
100%	100%	−22.0%	−9.6%	−5.3%	−43.5%	−8.6%

cost function in July reduces by 28%, and the nitrate RMS error reduces from 0.67 μg/m^3 to 0.44 μg/m^3. Using 10% (50%) representational error, the cost function reduces by 33% (26%), and the nitrate RMS error reduces to 0.43 μg/m^3 (0.45 μg/m^3). Repeating the regularization analysis and selecting a larger (smaller) γ_r would thus likely result in yearly results quite similar to those presented for a 30% representational error. After optimization, the yearly NMB for nitrate is −0.32 and for sulfate is −0.10. An unintentional consequence of specification of representational error as 30% of the measured value is that model overestimates contribute more to $\mathcal{J}$ than underestimates; as a result, the bias in the inverse modeling solutions is always less positive (or more negative) than the initial model bias. Perhaps a better estimate of representational error for future analysis would be similar to the mean normalized factor bias (Yu et al., 2006), wherein the error is considered to be 30% of $\boldsymbol{Hc}$ if $\boldsymbol{Hc}<\boldsymbol{c}_{obs}$ and 30% of $\boldsymbol{c}_{obs}$ if $\boldsymbol{Hc}>\boldsymbol{c}_{obs}$.

To explore the possibility that the local minimum found during the optimization is not the global minimum of $\mathcal{J}$, additional optimization tests can be performed starting with different initial guesses for the emissions scaling factors. To demonstrate, the optimization is repeated for July using a range of initial guesses for NH_3 emissions. The results from these tests are presented and analyzed in the following section.

4.5 Analysis of optimized emissions

4.5.1 Ammonia

The prior and posterior (optimized) emissions of NH_3 from anthropogenic sources are shown in Fig. 8. Scaling factors for emissions of NH_3 from other source sectors are shown in Fig. 9, though note the scale of the plots is magnified compared to Fig. 8. The overall result is a reduction in NH_3 emissions. The largest reductions occur sharply in the central

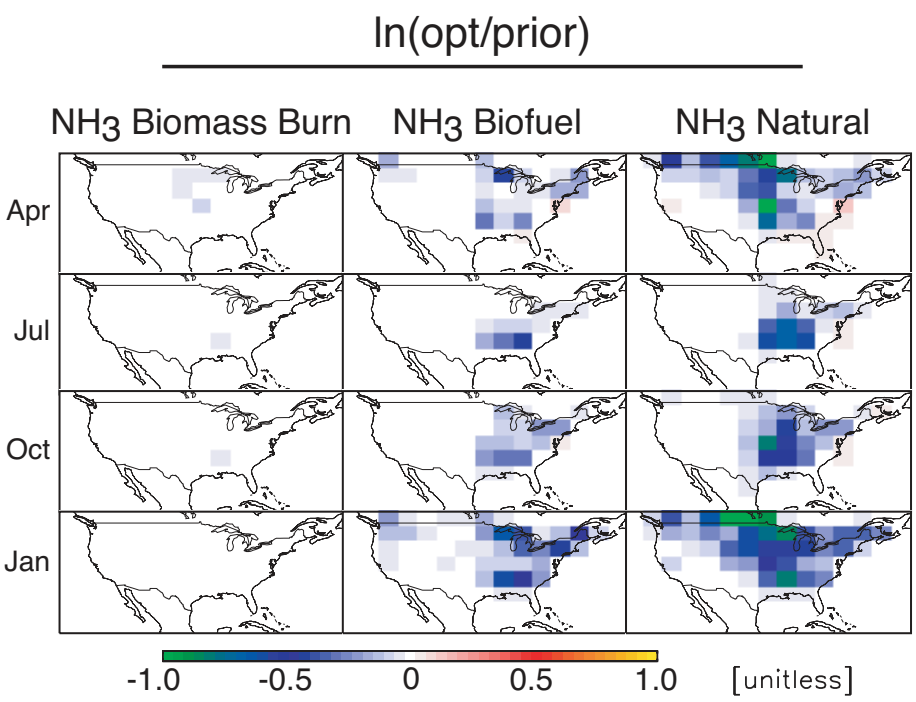

Fig. 9. Logarithmic scaling factors for NH_3 emissions from biomass burning, biofuel and natural sources.

Midwest during July and October, with decreases during January and April in the southern Midwest and, more broadly, throughout northern areas. There is also a small increase in anthropogenic NH_3 in California during spring, along eastern coastal areas in April, and in the Northeast during July. Emissions adjustments in individual locations cover a wide range of values, effectively altering the spatial distribution of NH_3 emissions. That the control parameters are assumed independent is an upper bound for this variability. The emissions of NH_3 in any place is simply the sum of the emissions from the individual source sectors. Given a spatially uniform adjoint forcing, the result would be a collective rescaling of NH_3 emissions that retains the original fractional distribution amongst the individual sectors. However, the adjoint forcing is not uniform so the fractional contribution to total NH_3 from the individual sectors changes. For example, the contribution to NH_3 emissions in the US from biomass burning, biofuel, anthropogenic sources, and natural sources in April is 1%, 8%, 64% and 27% in the prior model. After optimization, the contributions are 2%, 10%, 59% and 29%. Such reapportionment can be larger in individual locations. While the total emissions from each sector are decreased, the NH_3 emissions have been effectively redistributed amongst the sectors. The degree to which the resulting scaling factors for different sectors of the same chemical species are correlated is addressed in Sect. 4.5.3.

That the most significant difference between prior and optimized emissions scaling factors for any species considered is for NH_3 emissions is not an artifact of these emissions being ascribed the largest prior uncertainty, as it is true even when each type of emission is assumed a prior uncertainty of 100%, see Table 2. Hence, additional discussion of NH_3 emissions estimates is warranted. Emissions of NH_3 in the

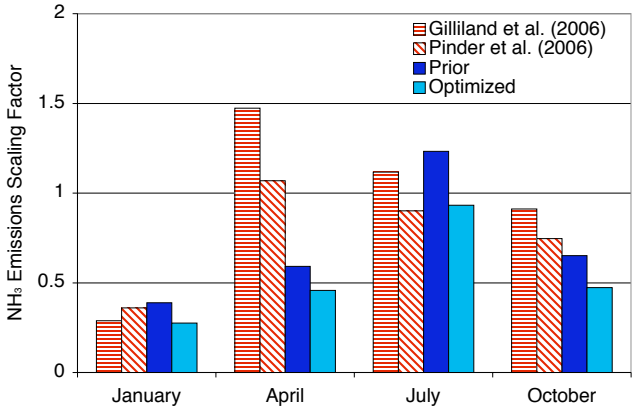

Fig. 10. Monthly emissions scaling factors for US emissions of NH_3 from all sources. Scaling is with respect to the NEI99 monthly value of 3.6 Tg N/yr. The initial GEOS-Chem simulation is shown in dark blue, with the optimized monthly scaling factors comprised of separate scaling factors in each grid cell are in light blue. The red striped bars show the inverse modeling estimates of Gilliland et al. (2006) (horizontal lines) and the process based estimates of Pinder et al. (2006) (diagonal lines). Note the modeling domain and prior emissions inventories for the latter two works are different than that of the present work.

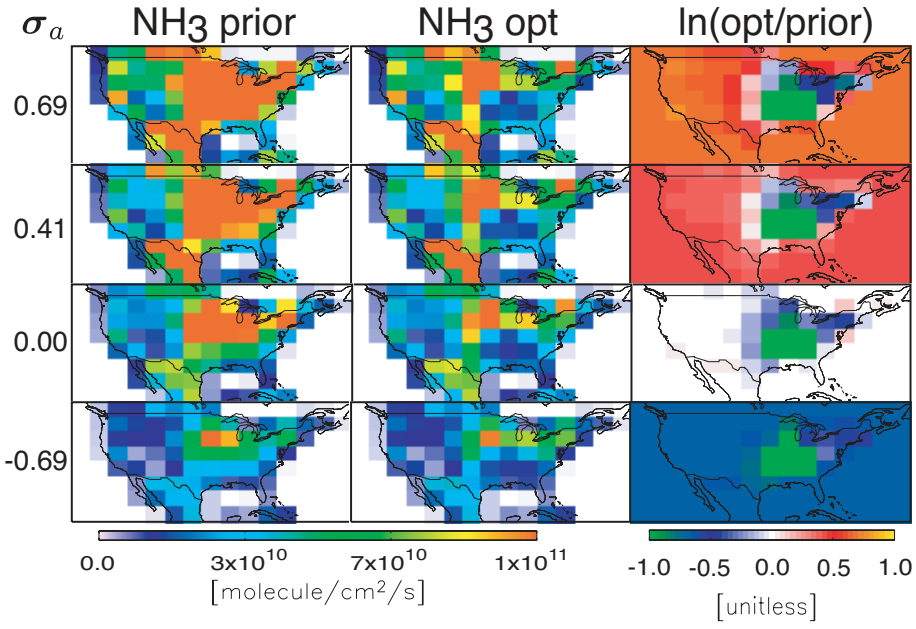

Fig. 11. Anthropogenic NH_3 emissions optimized using a range of initial emissions. On the left is the initial (prior) emissions inventory and its associated scaling factor, σ_a. In the center are the optimized inventories, and on the right are the optimized logarithmic scaling factors.

US have been analyzed in several recent studies (Gilliland et al., 2003, 2006; Pinder et al., 2006; Stephen and Aneja, 2008) and are cited as a significant source of model uncertainty (Yu et al., 2005; Nowak et al., 2006; Zhang et al., 2008). The inverse modeling efforts of Gilliland et al. (2003, 2006) focused on imparting seasonality to the aseasonal National Emissions Inventory (NEI) (EPA, 2001). Pinder et al. (2006) used a process-based approach to develop bottom-up NH_3 emissions for the Eastern US. Based on conclusions from Gilliland et al. (2006) that the NEI99 NH_3 inventory was still too high, Park et al. (2006) kept NH_3 emissions the same as in Park et al. (2004).

To compare with these previous works, results from the adjoint model-based inversion have been summarized as total adjustments to US NH_3 emissions. The total monthly values are shown in Fig. 10 as a percentage of the NEI99 constant monthly estimate of 3.6 Tg N/yr. Actual adjustments in the inversion were made at the inventory specific, model resolution level. The sum of all adjustments from the adjoint-based inversion results in a net reduction in total NH_3 emissions from the NEI99 monthly values. The results of the present work (blue) are compared to those from Gilliland et al. (2006) and Pinder et al. (2006) (red), noting that their monthly scaling factors shown in Fig. 10 have been adjusted to account for the fact that their basis is that of the NEI2001 inventory, which is 25% lower than the NEI99 inventory. For January, the aggregated inverse modeling results (light blue) are consistent with those of Gilliland et al. (2006) (horizontal stripes). The inversion of Gilliland et al. (2006) lead to an increase in April, while the present work estimates a decrease. In July, the present work estimated a value similar to that of the process-based estimates of Pinder et al. (2006), which is again opposite the direction of adjustments of Gilliland et al. (2006). Overall, the seasonal cycle of the adjoint-based inversion results matches that of Park et al. (2004), further supporting emissions estimates in which total NH_3 emissions peak in July rather than April, which is contrary to the emissions estimates of Pinder et al. (2006) and Gilliland et al. (2006). However, Pinder et al. (2006) do note that the process-based emissions inventory lead to overestimates of NH_x ($NH_x \equiv NH_3 + NH_4^+$) in April and underestimates NH_x in July compared to monthly average measurements in Pittsburgh, which may further support a peak in NH_3 emissions in summer rather than spring.

Figure 11 shows the optimization results for anthropogenic NH_3 emissions during the month of July using a range of initial guesses for NH_3 emissions. Results for the standard optimization (initiated with σ_a=0.0) are compared to results that begin with the following factors: σ_a=0.69, 0.41 and −0.69, which correspond to doubling, increasing by 50% and halving the emissions, respectively. The results demonstrate consistency of certain features across each optimization test. Most visibly, the scaling factors in the south-central US are always −1.0 or less. Scaling factors stretching from Michigan to New York are between −0.5 and −0.3, even when obtained by increasing emissions in those area from the test that began with σ_a=−0.69. While certain cells are estimated to have a positive scaling factor in some tests but negative scaling factors in other tests, the ranking of emissions adjustments in these cells relative to other

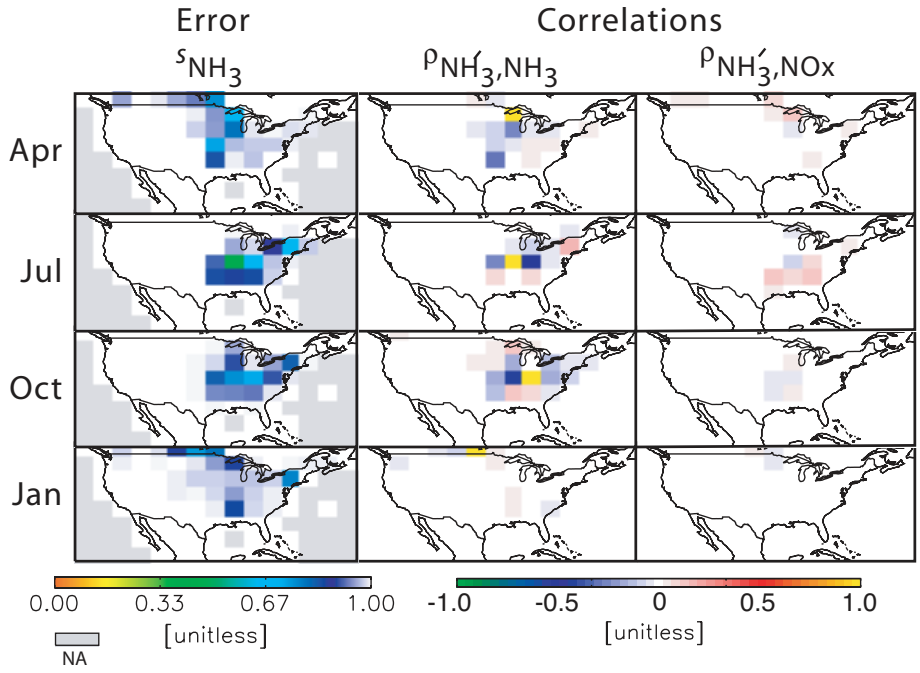

Fig. 12. The left column gives the standard error estimate of the optimized scaling factors for anthropogenic NH_3 emissions, s_{NH_3}. The center column shows the correlation of the scaling factor for anthropogenic NH_3 emissions with the least uncertainty (NH_3') with other scaling factors for the same inventory. The right column shows the correlation of the scaling factors for the anthropogenic NH_3 emissions with the least uncertainty (NH_3') with the scaling factors for surface emissions of NO_x.

areas within the same optimization test are mostly similar regardless of σ_a. Exceptions are locations such as Southern California, where emissions increased when σ_a=0.0 and σ_a=0.69 but not when σ_a=0.41. The final cost function is actually lowest for the σ_a=−0.69 test, for which $\mathcal{J}$=1366. The cost function for σ_a=0.0, 0.41 and 0.69 is 1469, 1615 and 1789, respectively. For the latter two tests, the total optimized US NH_3 emissions are greater than or equal the σ=0.0 emissions. For the σ_a=−0.69 test, the optimized US NH_3 emissions were 53% lower than the σ=0.0 emissions. Given the cost function values, it is most likely that the optimization results presented for σ_a=0.0 in July are an upper bound on total US NH_3 emissions, which may be even lower, but not likely higher. This is reasonable given that observed nitrate aerosol concentrations are typically very low during the summer. Any exception to that would require much higher NH_3 emissions, but any number of lower NH_3 emissions are plausible as long as the nitrate concentrations remain within the range of model and instrument uncertainty.

4.5.2 SO_x and NO_x

While the most substantial adjustments were made to NH_3 emissions, NO_x and SO_x emissions were also adjusted. As noted in Park et al. (2006), the NEI99 inventory compared to the prior inventory in GEOS-Chem has a change in total US anthropogenic NO_x emissions of −7.5% (from 6.7 from 6.2 Tg N/yr). For the base case, the inverse modeling results here indicate a small total change of −1.4% from all NO_x sources over the course of the year, see Table 2, most of which comes from changes to anthropogenic emissions. The tendency given looser constraints on NO_x emissions is greater reductions, as much as −9.6%. Remote sensing assessments of trends in NO_x emissions over the Eastern US also indicate reductions in NO_x (Kim et al., 2006; Stavrakou et al., 2008; van der A. et al., 2008) that may not be captured by the initial NO_x inventory, which at best represents NO_x levels three to four years prior to the observations. While US sulfur emissions in the NEI99 inventory are 9 Tg S/yr, compared to 8.3 Tg S/yr in the current model, recent revisions of inventories over Canada and Mexico are lower, from 2 and 1.9 down to 1.2 and 1.3 Tg S/yr (Park et al., 2006). Here we find SO_x inventories in the base case inversion essentially unchanged (−2.5 %). As mentioned in Sect. 4.4, this is partly a consequence of specifying tight constraints on SO_x emissions. The results of additional inverse modeling tests for different values of the assumed initial uncertainties in NO_x and SO_x emissions from anthropogenic sources are given in Table 2. When the constraints of the SO_x emissions are relaxed, there is a more significant reduction in the total yearly SO_x emissions. Also, the month to-month variations (not shown) for SO_x become very large using the 100% uncertainty inversion: the adjustments to total SO_x emissions range from −32.7% in April to 32.1% in July. In contrast,

when the initial uncertainty is 100%, adjustments to monthly total emissions of NO_x range from -3.6% in January to -14.5% in October, and adjustments to total NH_3 emissions range from -18.5% in July to -27.9% in January. Thus, the inversion of sulfate and nitrate observations gives the most robust constraints on NH_3 and, to a lesser extent, NO_x emissions.

4.5.3 Estimated uncertainty of optimized emissions

As noted in works such as Thacker (1989) and Müller and Stavrakou (2005), the inverse Hessian of the cost function, $\mathbf{IH}=\mathrm{Hess}(\mathcal{J})^{-1}$, is a linear estimate of the uncertainty of the optimized control parameters. Calculation of the full inverse Hessian ($M\times M$) itself being computationally prohibitive, low-rank estimates of the inverse Hessian can be generated from gradient-based minimizations of $\mathcal{J}$ by tracking successive changes from iteration i to $i+1$ in the control parameters, $\hat{\boldsymbol{\sigma}}_i=\boldsymbol{\sigma}_{i+1}-\boldsymbol{\sigma}_i$, and the gradients, $\hat{\boldsymbol{\lambda}}_{\sigma_i}=\boldsymbol{\lambda}_{\sigma_{i+1}}-\boldsymbol{\lambda}_{\sigma_i}$. In Müller and Stavrakou (2005), two different schemes for iteratively approximating **IH** were assessed for a study using the adjoint of a chemical transport model. The DFP algorithm was found to give better estimates of **IH** than the BFGS algorithm when compared to **IH** evaluated using finite differences. Based on their conclusions, the DFP algorithm is implemented, wherein **IH** is approximated as,

$$\mathbf{IH}_{i+1}=\mathbf{IH}_i+\frac{\hat{\boldsymbol{\sigma}}_i\hat{\boldsymbol{\sigma}}_i^T}{\hat{\boldsymbol{\lambda}}_{\sigma_i}^T\hat{\boldsymbol{\sigma}}_i}-\frac{\mathbf{IH}_i\hat{\boldsymbol{\lambda}}_{\sigma_i}\hat{\boldsymbol{\lambda}}_{\sigma_i}^T\mathbf{IH}_i}{\hat{\boldsymbol{\lambda}}_{\sigma_i}^T\mathbf{IH}_i\hat{\boldsymbol{\lambda}}_{\sigma_i}}, \quad (13)$$

where $\mathbf{IH}_0=\mathbf{S}_a$. The square root of the diagonal of **IH** are the estimated standard errors of the optimized scaling factors, $s_{\sigma_m}=(\mathrm{IH}_{m,m})^{\frac{1}{2}}$, where here the index m refers to elements m of the control vector and elements m,m of the inverse Hessian matrix.

The standard errors for the optimized emissions scale factors for the NH_3 emissions in each month are shown in Fig. 12. Starting from an assumed estimate of 100% error in the emissions[2], the error percent has decreased in locations where the scaling is nonzero, to as little as 50%. In general the largest error reductions occur where there is the most significant rescaling. For example, in July, the most significant scaling occurs in the same place as the greatest error reduction. However, the greatest error reduction is one grid cell to the east of the most significant scaling in October. The reduction in uncertainty appears similar from month-to-month, indicating that measurements of sulfate and nitrate may provide year-round constraints on NH_3 emissions. A subtle but crucial point in interpreting values of s_{σ_m} is that Eq. (13) is an approximation to **IH** that is limited to information gleaned from minimization of $\mathcal{J}$. Since this minimization proceeds along the direction of the largest contributions to the model prediction error, the estimate of **IH** does not contain much information on parameters whose influence on $\mathcal{J}$ is minimal because they affected model concentrations that either agreed with observations or did not coincide with any observations. The full Hessian is required to completely determine the power of the observations to resolve the model parameters (Tziperman and Thacker, 1989).

Also shown in Fig. 12 are error correlations, which for two scaling factors σ_{m_1} and σ_{m_2} are computed as

$$\rho_{\sigma_{m_1},\sigma_{m_2}}=\frac{IH_{m_1,m_2}}{(IH_{m_1,m_1}IH_{m_2,m_2})^{\frac{1}{2}}}.$$

As the initial estimate of $\mathbf{S}_a$ is diagonal, nonzero correlations between two scaling factors indicate that these factors are not independently constrained by the observations during the inversion. The correlation between most pairs of parameters is near zero, particularly for pairs of parameters whose values were relatively unchanged during the optimization. However, definite correlations become evident for parameters whose values were rescaled during the inversion. In both the center and right columns of Fig. 12, correlations are shown with respect to the most certain parameter, $\sigma_{\mathrm{NH}_3'}$, identified from the minimum of the plot in the left column of each row. The panels in the center column show the correlation of $\sigma_{\mathrm{NH}_3'}$ with those of the scaling factors for anthropogenic NH_3 emissions in other locations. The error correlation of $\sigma_{\mathrm{NH}_3'}$ with other σ_{NH_3} usually has a strong negative correlation nearby. This anti-correlation between neighboring grid cells is an indication that the mixing of NH_3 emitted from the neighboring cells is collectively influencing $\mathcal{J}$ in a non-separable fashion.

The right column of Fig. 12 shows correlation of $\sigma_{\mathrm{NH}_3'}$ with scaling factors for surface emissions of NO_x in other locations. In these locations in each month, the largest component of the adjoint forcing comes from overestimation of NO_3^-. In April and January, emissions of NO_x and emissions of NH_3 both favor formation of NO_3^- in the form of NH_4NO_3, hence their emissions are positively correlated. However, co-located emissions of NO_x have a strong negative correlation with $\sigma_{\mathrm{NH}_3'}$ in July and October. When NH_4^+ is predominantly in the form of $(NH_4)_2SO_4$, and the amount of NO_3^- is only from NH_4NO_3 that forms when there is a surplus of NH_3 (as $(NH_4)_2SO_4$ formation takes precedence over NH_4NO_3 in warmer, dryer conditions), the consequence of NO_x emissions can be to reduce the amount of surplus NH_3 by increasing the amount of SO_4^{2-}, thereby reducing the formation of NH_4NO_3. Therefore, the scaling factors for emissions of NO_x and NH_3 can be anti-correlated under certain conditions.

Correlations between emissions of different species in the same location are generally small, between -0.2 and 0.2, and vary between positive and negative values depending upon

[2]Note, if parameter p_a has a prior fractional error of x, then the absolute parameter error is $s_{p_a}=xp_a$, and the error in the scaling factor $\sigma=ln(p/p_a)$ is $s_\sigma=s_{p_a}/p_a=x$. Hence, a fractional error in p_a is the same as the absolute error in σ, and, conversely, the error in the estimated parameters are $s_p=ps_\sigma$.

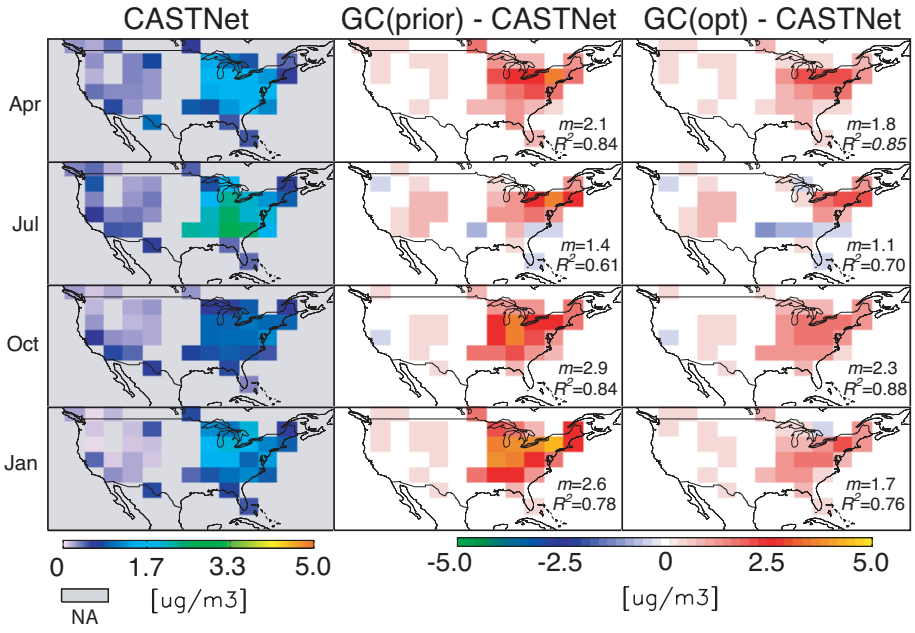

Fig. 13. CASTNet observations of monthly average surface level NH_4^+ concentrations (averaged on the GEOS-Chem model grid) are shown in the left column for each month. Also shown is the difference between these observations and the GEOS-Chem model estimates based on the original emissions inventories (center) and the optimized emissions inventories (right). The numbers in the corner of the difference plots are coefficient, m, and R^2 for regression through the origin.

the local chemical conditions. However, the adjustments to the emissions of a given species are correlated to adjustments of the same species from a different sector in the same location. In general, such correlations are negative, range between 0 and -0.5, and are strongest for NH_3 from anthropogenic sources with NH_3 from natural sources. The magnitude of the anti-correlations indicates the degree to which the observations have constrained total NH_3 emissions, but can not distinguish between source sectors. Hence, the inverse modeling solution does not give entirely independent estimates of the contributions from different source sectors for a given species.

4.6 Comparison to CASTNet NH_4^+

Inverse modeling using NH_4^+ observations alone may not provide robust constraints on NH_3 emissions (Pinder et al., 2006). However, as a check of the inverse model results using sulfate and nitrate observations, measurements of NH_4^+ from the CASTNet network (Baumgardner et al., 2002) are compared to model estimates using both the prior emissions inventory and the optimized emission scaling factors from Sect. 4.4. In Fig. 13, the left column displays the observations, averaged onto the GEOS-Chem grid, while the center and right columns show the difference between the model and the observations using the prior and optimized emissions inventories. From a visual comparison, it is evident that estimates of NH_4^+ are largely improved throughout the Midwest, while the predictions are persistently high in the Northeast. Panels in the latter columns also contain the slopes and R^2 values of regressions through the origin. Using the optimized emissions inventory brings the regression coefficients closer to unity for all months and captures more of the variance of the observations in all months except January. Overall, changes in estimated NH_4^+ from inversion of sulfate and nitrate observations are in a direction consistent with independent CASTNet observations. Though total performance is worst in October, improvement is shown in each month, indicating the year-round potential of inverse modeling based on sulfate and nitrate observations to constrain NH_3 (and hence NH_4^+).

In Park et al. (2004), seasonally-averaged model estimates are compared to CASTNet NH_4^+ using nearly the same version of GEOS-Chem as the prior estimates in the present study, though at a finer resolution ($2^\circ \times 2.5^\circ$). In Park et al. (2006), the model is again compared to CASTNet NH_4^+, this time using a nested $1^\circ \times 1^\circ$ simulation with updated SO_x and NO_x emissions, though NH_3 emissions are the same as Park et al. (2004) and the prior estimates of the present work. The overall agreement between estimated NH_4^+ and the CASTNet observations is markedly improved between Park et al. (2004) and Park et al. (2006). The prior and optimized models in the present work are not as good as the seasonally averaged comparisons in Park et al. (2004) or Park et al. (2006). That Park et al. (2004) considered seasonal averages, rather than monthly averages, likely contributes to better apparent agreement with CASTNet. Some of the discrepancy of the

present work may also be owing to the coarse model resolution. As the number and distribution of subgrid observations are not uniform, agreement is expected to improve using a finer resolution simulation. Comparing the results using the prior emissions in the present work with Park et al. (2004), the estimated resolution error of 30% may be underestimated.

5 Nonattainment influence maps

In the second stage of this work, the observationally constrained model is used to assess the influence of aerosol precursor emissions on $PM_{2.5}$ air quality metrics. Previous works have highlighted how $PM_{2.5}$ air quality attainment may be complicated by the interactions between the inorganic species. The nonlinear relationship between sulfate and total $PM_{2.5}$ mass has been noted to reduce effectiveness of SO_x control in colder seasons (West et al., 1999; Vayenas et al., 2005). Pinder et al. (2007) examined the tradeoffs between SO_x controls and NH_3 controls in the Eastern US during two weeks of 2002 though a matrix of simulations applying uniform changes throughout the model domain to total emissions SO_x, NO_x and NH_3. Based on a combined analysis of chemical effectiveness and the cost of SO_2 emissions controls, Pinder et al. (2007) demonstrated the effectiveness of abatement of SO_2 emissions over NH_3 emissions in July and the reverse in January. In the present work, we use adjoint sensitivities to explore the effectiveness of incremental changes to emissions from tens of thousands of individual emissions locations and sectors on both peak concentrations and ambient levels of the modeled inorganic component of $PM_{2.5}$.

5.1 Peak $PM_{2.5}$ episodes

The model response is now defined as a representative metric of nonattainment for peak aerosol concentrations,

$$\mathcal{J}_a = \frac{1}{2} \sum_{i \in \mathrm{US}} \sum_{\mathrm{day}\ j} \theta(a_{i,j}) a_{i,j}^2, \tag{14}$$

where

$$a_{i,j} = \left(\sum_{\hat{k}} \bar{c}_{i,j,\hat{k}} \right) - \bar{c}_a, \quad \hat{k} = \{SO_4^{2-}, NO_3^-, NH_4^+\},$$

with $\bar{c}_{i,j,\hat{k}}$ being the 24 h average model estimated aerosol concentration of species $\hat{k}$ in location i on day j, and θ is the following simple function,

$$\theta(a) = \begin{cases} 0 & a \le 0 \\ 1 & a > 0 \end{cases}.$$

The air quality threshold is $\bar{c}_a$, taken to have a value of $10\,\mu g\,m^{-3}$. Although this threshold is much lower than the actual 24 h NAAQS of $35\,\mu g\,m^{-3}$, here carbonaceous aerosol has not been included in the set of active species, $\hat{k}$, and the coarse model resolution is not expected to represent the magnitude of localized maximums during acute pollution episodes. To compensate, the metric is squared (i.e., it is an L_2 norm) to emphasize episodes of peak concentrations, which are of most concern for exceedences of daily air quality standards.

The nonattainment metric is evaluated for each of the four months considered, and the results are shown in Fig. 14. In the left column is the average contribution to the nonattainment metric from each of the aerosol species. This is essentially the adjoint forcing, where the forcing is divided in each cell by the number of days for which concentrations in that cell exceeded the threshold. These plots display the regions in which the 24 h average aerosol concentration at some point during the month was in the nonattainment regime (θ=1). Throughout the year, the only regions of nonattainment are in the Eastern US. This is likely owing to the model resolution, which is not well suited for assessing pollution episodes in the Western US that are likely to be much more localized. For each month, the different rows in Fig. 14 show the contribution to nonattainment from the individual aerosol species. In April, July, and October, SO_4^{2-} dominates the peak concentrations. NO_3^- plays a significant role in October and January, while NH_4^+ contributes fairly consistently throughout the year.

Column (b) of Fig. 14 shows emissions of SO_x, NO_x and NH_3, each given as a percent of the total emissions for each species in the US. This includes contributions from each of the source sectors listed in Table 1. Column (c) shows the semi-normalized sensitivities of the cost function with respect to emissions of each of these species, shown as a percent, $\frac{\partial \mathcal{J}_a}{\partial p_i} \frac{1}{\mathcal{J}_a} \times 100\%$, where p_i is the total emissions of a chemical species in location i. These are referred to as nonattainment susceptibilities, as they indicate the per-unit-emissions influence of emissions of a particular species on nonattainment, regardless of the current value of the emissions (except in the case that emissions are zero, for which the sensitivities are not defined). Column (d) shows the fully normalized sensitivities, $\frac{\partial \mathcal{J}_a}{\partial p_{i,m}} \frac{p_{i,m}}{\mathcal{J}_a} \times 100\%$, where $p_{i,m}$ is an emission from a specific source sector m in location i. Here we show only the normalized sensitivities for the sectors with the greatest influence for each species. For small perturbations, these normalized sensitivities give an estimate of the percent change in the cost function per fractional change in emissions, $\frac{\triangle \mathcal{J}_a / \mathcal{J}_a \times 100\%}{\triangle p_{i,m} / p_{i,m}}$. Thus, these sensitivities are first order approximations of the effectiveness of specific emissions changes on affecting nonattainment. The nonattainment sensitivities in (d) are likely valid over a modest range of emissions perturbations commensurate with typical emissions abatement strategies (10–30%). Over this range, the most significant sensitivities for the aerosol species considered here have been shown to be robust (Henze et al., 2007; Koo et al., 2007). For the following discussion, it is

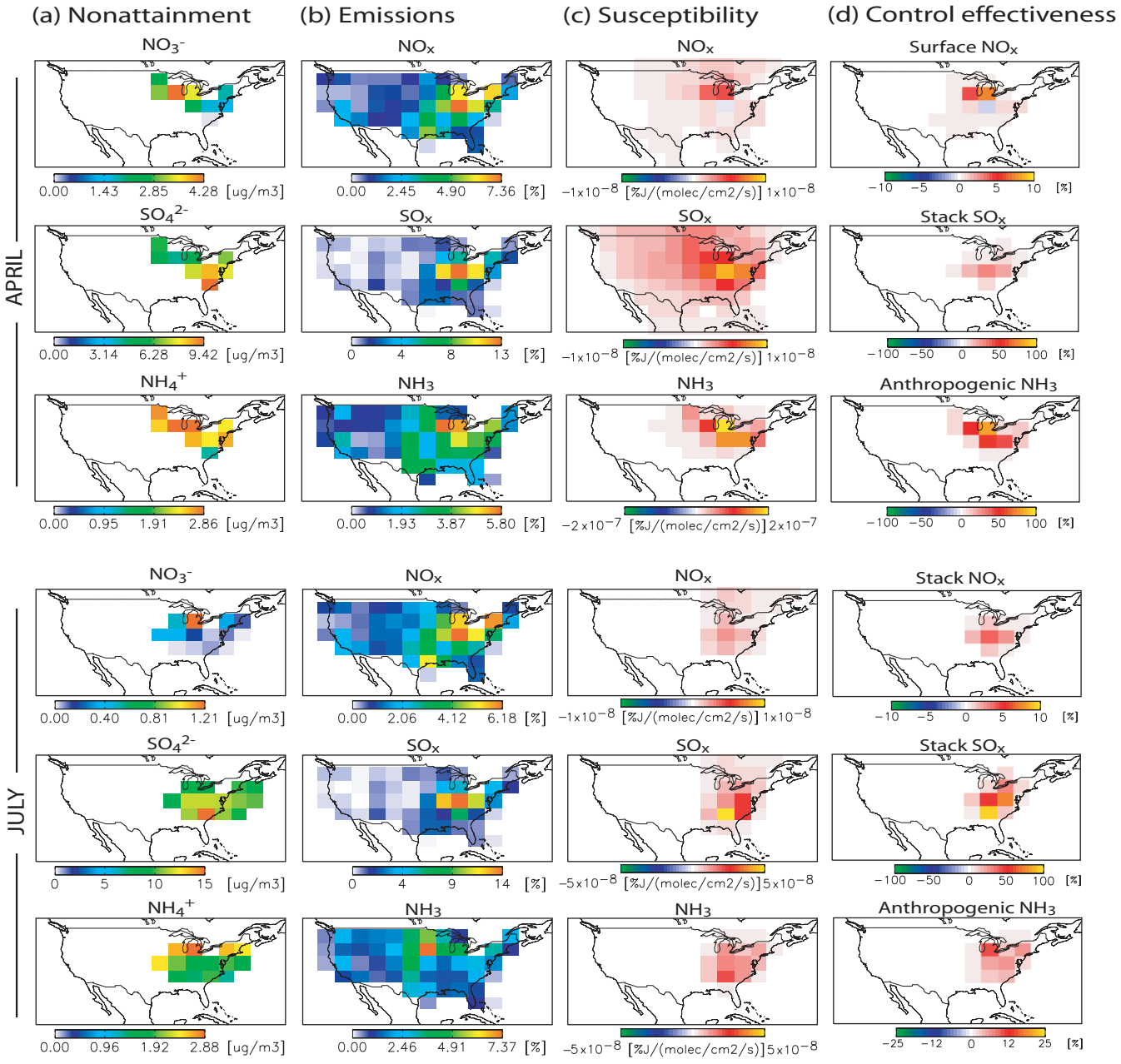

Fig. 14. Peak aerosol nonattainment analysis showing **(a)** average contribution from each aerosol species to the nonattainment metric, $\mathcal{J}_a$, **(b)** emissions of aerosol precursors normalized with respect to total US emissions, **(c)** the susceptibility of the nonattainment with respect to emissions of aerosol precursors, p_i (i.e., semi-normalized sensitivities, $\frac{\partial \mathcal{J}_a}{\partial p_i}\frac{1}{\mathcal{J}_a} \times 100\%$), and **(d)** the effectiveness of incremental controls of emissions from specific sectors, $p_{i,m}$, on reducing nonattainment (i.e., normalized sensitivities, $\frac{\partial \mathcal{J}_a}{\partial p_{i,m}}\frac{p_{i,m}}{\mathcal{J}_a} \times 100\%$). Model simulations use the optimized emissions estimates from Sect. 4.4.

important to note the variations in the scale of the nonattainment sensitivity plots. Also note the magnitudes of NO_x, SO_x and NH_3 emissions are typically in the range of 10^{10}–10^{12} molec/cm^2/s.

The combination of the four plots in each row of Fig. 14 maps the influence of inorganic $PM_{2.5}$ precursor emissions on attainment in a manner that is well suited for informing decision making concerning emissions abatement (Hakami et al., 2006). The distribution of nonattainment, column (a), shows locations that will benefit from implementation of emissions regulations that enforce air quality attainment. The distribution of the emissions, column (b), shows the areas that would be most heavily burdened by any simple emissions abatement strategy based on absolute emissions caps,

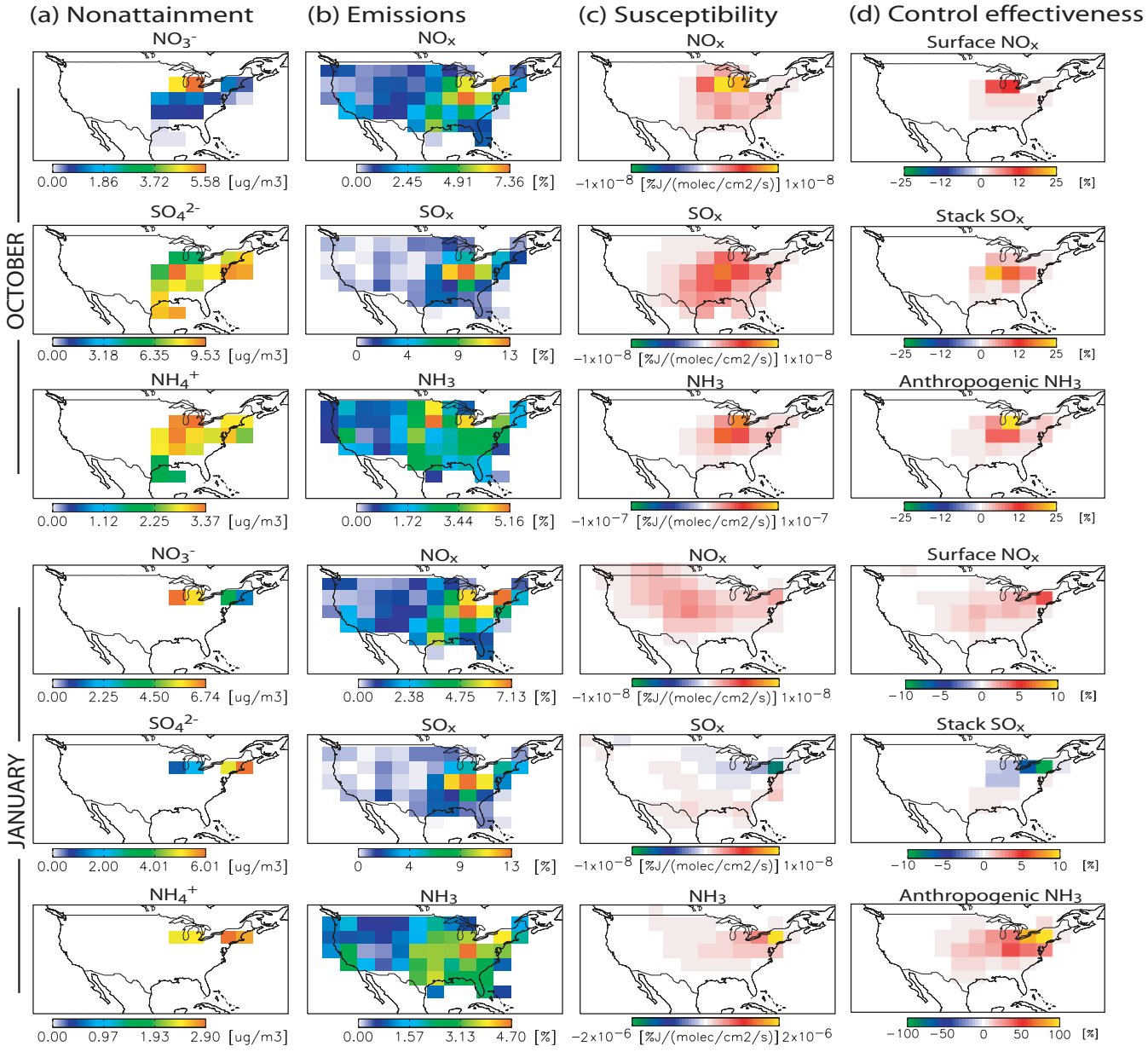

Fig. 14. Continued.

while the nonattainment sensitivities in column (d) show locations where reducing existing emissions would actually be the most effective towards achieving air quality attainment. The maps in column (c) indicate regions where nonattainment is most susceptible to total emissions changes, indicating areas where introduction of new sources (e.g., owing to land use changes) would have the largest consequence even if current emissions are small. The disparity between the maximums in these types of plots concisely depicts the challenges in designing regulation measures to control long-lived secondary pollutants. For example, consider the results for the month of July. While the bulk of the NH_3 is emitted in the northern Midwest, it is sources of NH_3 in the Eastern US that ultimately most substantially influence nonattainment. Sources of NH_3 in the latter regions are co-located with sources of SO_x, leading to more aerosol formation per emitted NH_3. Additionally, the nonattainment is most susceptible to emissions in the Southeast. In October and January, the effectiveness of anthropogenic NH_3 controls are again linked to the locations of the SO_x emissions, with peak effectiveness and susceptibilities consistently east of peak emissions. In general, it is evident from the spatial disparities noted between maximums in columns (b) and (d) that regulating emissions near the largest sources can sometimes have only minimal benefits for air quality attainment.

For each month, it is also interesting to compare the effectiveness of reductions in one emitted species vs another. In April, nonattainment is 20 times more susceptible to NH_3 emissions than stack SO_x emissions, and peak anthropogenic NH_3 emissions are by far the most effective targets for control. In July, controls of stack SO_x are more effective than control of anthropogenic NH_3. In October, although nonattainment is nearly 10 times more susceptible to NH_3 emissions, anthropogenic NH_3 controls are more effective than stack SO_x controls in some locations, and vice versa in others, owing to the magnitude of the emissions from these sectors. The effect of surface NO_x controls is much weaker than either anthropogenic NH_3 or stack SO_x controls in April, and much weaker than stack SO_x controls in July. Despite the susceptibility to NO_x emissions being about five times less than that of anthropogenic NH_3 controls in July, effectiveness of their controls are similar in magnitude. In October, surface NO_x controls are more effective than either stack SO_x controls or anthropogenic NH_3 controls in northern locations. The susceptibility to NO_x emissions is also much more focused in October as opposed to January, where the NO_x susceptibility is much more diffuse, even though the non-attainment is highly focused. This may indicate the difference between immediate formation of NO_3^- from NO_x vs a more delayed and diffuse influence following NO_x sequestration as peroxyacetyl nitrate (PAN).

In January, anthropogenic NH_3 controls dominate by a factor of 10, and susceptibility to NH_3 emissions is nearly 200 times larger than for SO_x or NO_x. Reducing SO_x, and hence sulfate, is rendered ineffective owing to rapid replacement of SO_4^{2-} by NO_3^-, formation of the latter being favored by colder temperatures. This effect is so extreme that during the winter, the nonattainment sensitivity of SO_x emissions has a value near the nonattainment region that is actually negative. If removal of sulfate aerosol in the presence of fixed total ammonia and nitric acid concentrations cause one mole of $(NH_4)_2SO_4$ (molecular weight=132) to be replaced by two moles of $(NH_4)NO_3$ (molecular weight=80), then the total $PM_{2.5}$ concentration would be enhanced by decreases in SO_x emissions. Also, NO_x controls can potentially be counterproductive in April (the mechanisms for such a feedback is given in Sect. 4.5.3), though the overall magnitude of the latter effect is small. The existence of such feedbacks have been noted previously (Napelenok et al., 2006; Henze et al., 2007); here the explicit consequences for air quality attainment are quantified.

So far the influences of emitted species have been considered only for the most influential source sector. The fully normalized sensitivities, $\lambda_{p_{i,m}} = \frac{\partial \mathcal{J}_a}{\partial p_{i,m}} \frac{p_{i,m}}{\mathcal{J}_a}$, estimate how changes to emissions from sector m in location i will influence the air quality metric. Since the spatial distributions of emissions in different sectors are not the same, the consequence of changing all emissions for a given species by a certain amount will be different from sector to sector. Naturally, a significant component of this sector-to-sector difference is owing to the difference in magnitudes of the emissions from different sectors. To distinguish between these effects, the following statistic is calculated,

$$\chi_m = \left(\frac{|\sum_i \lambda_{p_{i,m}}|}{|\sum_{i,m} \lambda_{p_{i,m}}|} - \frac{\sum_i p_{i,m}}{\sum_{i,m} p_{i,m}} \right) \times 100\%, \quad (15)$$

where here i is the spatial index and m is the index of a specific source sector. For the summations, the range of the spatial index i is the physical range over which emissions from sector m have at least a 0.001% effect on $\mathcal{J}$ (i.e., $|\lambda_{p_{i,m}}| > 10^{-5}$). The sum over m is for all the source sectors for a given chemical species, listed in the rows of Table 1. The values for χ_m are presented in Table 3. Overall, χ_m indicates the net relative importance of an emission from a particular sector relative to the magnitude of the emission from that sector. For example, in July, stack NO_x emissions are 23% of the total NO_x emissions from all sources, and the sensitivity with respect to stack NO_x emissions is 43% of the sensitivity with respect to NO_x emissions from all sources. From Eq. (15), $\chi_{NO_x,stack}$=26%, which means a change to emissions of NO_x from industrial sources is 26% more effective in reducing nonattainment than in reducing the total amount of NO_x emitted. Therefore, abatement strategies targeting NO_x from stack emissions are estimated to be much more effective than strategies that target NO_x emissions as a whole. Such findings are generally robust over the course of the year, as the signs of the χ_m are consistent from month to month. Overall, emissions of SO_x and NO_x from industrial stacks are much more critical than emissions from the transport sector. Emissions of NH_3 from natural and biofuel sources are more important than anthropogenic NH_3 emissions. Emissions such as NO_x from lightning and soil, SO_x from shipping and NH_3 from biomass burning are not as influential for

Table 3. Precent by which changes to emissions of a given species from particular sectors are more effective for reducing nonattainment than changes to emissions of that species from all sectors (Eq. 15).

Emission sector	January	April	July	October
SO_x surface	−11	−14	−11	−12
SO_x stack	16	17	13	13
SO_x shipping	−4	−2	−2	−1
NH_3 anthropogenic	−10	−11	−16	−23
NH_3 natural	9	11	12	14
NH_3 biomass burning	−18	−9	−3	0
NH_3 biofuel	18	9	8	10
NO_x surface	−2	−4	0	−6
NO_x stack	13	11	26	14
NO_x lightning	−6	−5	−19	−6
NO_x soil	−4	−2	−8	−2

Table 4. The influence of specific emissions sectors on daily average inorganic $PM_{2.5}$ concentrations. The total integrated percent influence is presented (Total) along with a breakdown of this total into contributions from spatial regions (ROW=rest of world).

Emission sector	Total	Percent from each region			
		US	Canada	Mexico	ROW
SO_x surface	11.1	57.8	8.2	23.9	10.1
SO_x stack	30.1	75.1	16.7	3.4	4.7
SO_x shipping	2.0	67.9	6.9	6.4	19. 9
SO_x biomass burning	0.2	16.2	1.1	77.3	5.4
SO_x biofuel	0.03	2.9	25.4	36.1	35.6
NH_3 anthropogenic	19.6	90.0	6.0	2.3	1.7
NH_3 natural	9.2	89.4	8.4	0.1	1.3
NH_3 biomass burning	0.6	60.1	2.3	33.3	3.1
NH_3 biofuel	3.5	95.4	3.9	0.4	0.2
NO_x surface	6.7	84.4	5.3	8.3	2.0
NO_x stack	2.7	97.7	1.1	0.4	0.8
NO_x lightning	0.1	68.3	1.1	24.3	6.2
NO_x soil	0.7	65.3	4.1	28.8	1.7

nonattainment owing to their spatial and temporal distributions.

While the present work considers only the contribution of inorganic species to $PM_{2.5}$, it is important to keep in mind the role of additional species. When excess NH_3 is present, the sensitivity of HNO_3 with crustal mineral species can be relatively low, at times an order of magnitude less than the sensitivity of nitrate aerosol to NH_3 (Fountoukis et al., 2009). However, in areas where NH_3 levels are lower and mineral concentrations higher, the importance of NH_3 in governing nitrate formation may be diminished. Hence, the nonattainment sensitivities with respect to NH_3 emissions may be exaggerated in the Southwest owing to local dust sources or in the western US owing to transpacific dust transport in the springtime. Still, most of the sensitivities for the present study were located in the central and eastern US. Primary and secondary organic aerosol are also important for determining total levels of $PM_{2.5}$. While SOA formation in the winter is not as significant as other seasons, the potential for sulfate to enhance SOA formation (e.g., Surratt et al., 2007) may increase the effectiveness of SO_x controls for total $PM_{2.5}$ in other seasons. Observed dependence of secondary organic aerosol on aerosol water content (Hennigan et al., 2008, 2009; Volkamer et al., 2009) suggest additional pathways by which deliquesced inorganic aerosol could affect total particulate mass. Internal mixing of aerosols can also lead to a relationship between primary carbonaceous aerosol and sulfate by altering the lifetime of the agglomerated particles with respect to wet scavenging (Stier et al., 2006). Finally, it is again noted that the nonattainment modeled here is only representative given the current model resolution and exclusion of carbon aerosol. Detail assessment of nonattainment regions will require high resolution nesting, or coupling of the global adjoint model with regional scale adjoint models. Model responses should also be considered that separately address individual $PM_{2.5}$ components, which may have different consequences for public health (Reiss et al., 2007). These are important topics for future consideration.

5.2 Long-range influences

Episodes of pollution transport from East Asia have been repeatedly observed to contribute to $PM_{2.5}$ concentrations in the Western US (e.g., Jaffe et al., 2003). Several modeling studies of have been performed to provide further characterization of such influences, using methods such as tagged tracers (Benkovitz et al., 2006; Liu et al., 2008) or emissions toggling (Park et al., 2004; Heald et al., 2006a; Chin et al., 2007). Results consistently show that while emissions from East Asia are not likely affecting $PM_{2.5}$ NAAQS attainment, there is a noticeable intercontinental contribution ($\sim 1\,\mu g/m^3$) on background concentrations, particularly in the Western US. This has implications for attainment of regional haze rules (Park et al., 2004, 2006), and intercontinental influences may be more important at higher altitudes owing to their climate impacts (Chin et al., 2007). There is also evidence that the mortality response with respect to surface level $PM_{2.5}$ concentrations persists well below current air quality thresholds (Schwartz et al., 2002, 2008), so such influence may yet be of concern for public health.

The classes of source regions considered in modeling studies of long-range transport are often quite broad, such as all emissions from all sectors, tagged according to a continental scale region. In contrast to previous work, the adjoint modeling approach used here distinguishes the effects from different emitted species, sources, and source locations. In addition to the long-range influence of SO_x emissions on sulfate, here the influence of NH_3 and NO_x on the total mass of the sulfate- ammonium-nitrate aerosol are also considered using the following model response,

$$\mathcal{J}_{a,\infty} = \sum_{i \in \mathrm{US}, \mathrm{day}\ j} a_{i,j}, \tag{16}$$

where $a_{i,j}$ is defined as in Eq. (14), except now $\bar{c}_a$=0. Thus, sensitivities with respect to $\mathcal{J}_{a,\infty}$ show which emissions influence 24 h aerosol concentrations in the United States.

Results from the single adjoint model run are summarized in Table 4, where the adjoint sensitivities are integrated over the following four regions: contiguous US, Canada, Mexico and Central America, and the rest of the world (ROW). The largest influence for each of the sectors shown here is from the local (i.e., US) emissions. Other sectors (such as biomass burning and biofuel), have a major influence from abroad, but the overall magnitudes are much smaller. The emissions sector with the largest transboundary influence is that of surface emissions of SO_x, largely because local emissions from this source within the US domain are relatively small. The sensitivities with respect to $\mathcal{J}_{a,\infty}$ are shown in Fig. 15. The plot scales are purposefully capped at low values to highlight

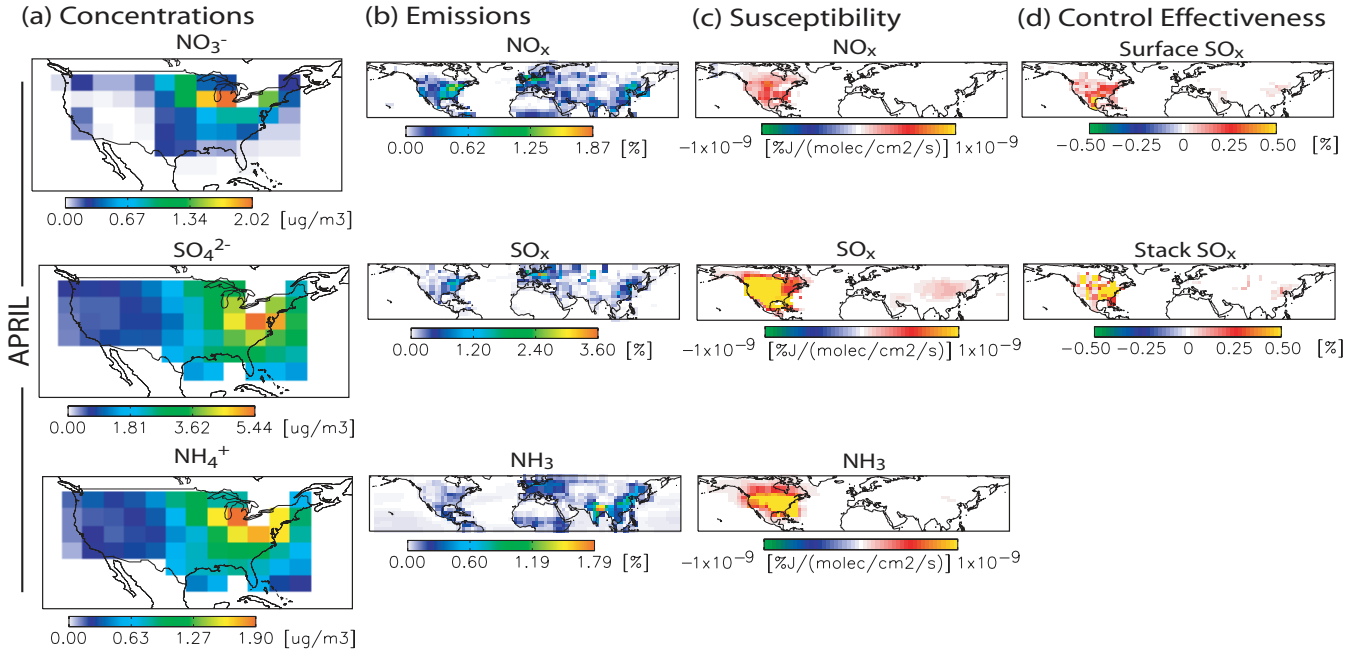

Fig. 15. Long-range nonattainment analysis showing **(a)** the 24 h average inorganic $PM_{2.5}$ concentrations, **(b)** anthropogenic emissions of SO_x and NO_x, **(c)** the semi-normalized sensitivities $\left(\frac{\partial \mathcal{J}_{a\infty}}{\partial p_i}\frac{1}{\mathcal{J}_{a\infty}}\right)$ with respect to emissions in location i and **(d)** the normalized sensitivities $\left(\frac{\partial \mathcal{J}_{a\infty}}{\partial p_{i,m}}\frac{p_{i,m}}{\mathcal{J}_{a\infty}}\right)$ with respect to emissions in location i from sector m.

contributions from outside the US. The only intercontinental emissions that the daily average concentrations are susceptible to are those of SO_x, hence only the control effectiveness of the SO_x emissions are shown. Sensitivity with respect to NO_x emissions may be underestimated as the model does not account for aerosol nitrate associated with transpacific dust transport (Malm et al., 2004; Fairlie et al., 2007). From these figures is evident that the main contribution to ROW comes from eastern China, with some contribution from emission in the Middle East.

6 Conclusions

The adjoint of the chemical transport model GEOS-Chem (Henze et al., 2007) is applied to evaluate sources of secondary inorganic aerosol throughout the US. Using the 4D-Var framework, the forward model parameters are constrained using measurements of sulfate (SO_4^{2-}) and nitrate (NO_3^-) aerosol from the IMPROVE network of monitoring stations (Malm et al., 1994) during the months of April, July and October of 2001, and January of 2002. Significant discrepancies exist for initial model estimates of NO_3^- compared to the observations. The adjoint model is used to select variable model parameters that most significantly influence this discrepancy. Parameters initially considered include scaling factors for emissions of SO_x, NO_x, and NH_3 from several source sectors, initial conditions of all tracers, and heterogeneous uptake coefficients. Anthropogenic emissions of NH_3 are found to be most influential, followed by natural emissions of NH_3, anthropogenic stack emission of SO_x, and surface emissions of NO_x. This finding is consistent with recent studies that indicate NH_3 emissions are highly influential in determining the total concentration of inorganic $PM_{2.5}$ and are themselves highly uncertain (Yu et al., 2005; Gilliland et al., 2006; Pinder et al., 2006; Nowak et al., 2006; Zhang et al., 2008; Wu et al., 2008; Beer et al., 2008).

Inverse modeling of sulfate and nitrate using the adjoint model affords optimization of the emissions at a resolution commensurate with that of the forward model itself. Overall, the optimized emissions inventories are adjusted most significantly for NH_3 emissions, which are largely reduced in the East and Midwest. There is considerable variability in the rescaling of emissions from different source sectors in different locations, which effectively changes the spatial distribution of the emissions, and also the distribution of emissions amongst individual emissions sectors. For example, while the total US NH_3 emissions from each sector are reduced, the resulting fraction of NH_3 emissions from anthropogenic sources throughout the US is 5% less than in the initial inventory, with changes as large as 20% in individual locations. The consequence of using the constrained emissions inventories is a significant improvement to the nitrate simulation, reducing the root mean squared error by 43%. The absolute normalize mean bias is reduced by 20%,

though underestimation of nitrate aerosol persists throughout the West in April, July and October. The resulting magnitude of the total NH_3 inventory is similar to that found in Gilliland et al. (2006) for January, but much lower in April, July and August. The total NH_3 emissions agree with Pinder et al. (2006) in July, while overall, the seasonal cycle is that of Park et al. (2004), with NH_3 emissions peaking in July rather than April.

Inverse modeling tests are conducted for a range of assumptions concerning the prior uncertainty of the emissions. The anthropogenic emissions of NO_x and SO_x are initially assumed to be much more certain than emissions of NH_3; hence, the inverse modeling estimates of emissions of NO_x and SO_x are more tightly constrained to the initial inventory. As these constraints are loosened, the nitrate simulation remains largely unaffected. When all emissions are assumed to be equally uncertain, the solution for the SO_x emissions exhibits large month-to-month fluctuations, while the total yearly changes to SO_x and NO_x are still not as significant as the NH_3 changes. Changes in anthropogenic NO_x emissions of -1% to -10% (for assumed uncertainty in NO_x emissions of 30% to 100%, respectively) from the original inventory based on 1998 activity levels are consistent with recent revisions to the anthropogenic NO_x inventory used by GEOS-Chem of -7.5% (Park et al., 2006) and with remotely observed decreases in NO_x emissions in the eastern US over the last decade (Kim et al., 2006; van der A. et al., 2008; Stavrakou et al., 2008). Inverse modeling estimates of NH_3 emissions are found to be relatively invariant to assumed uncertainties of NO_x and SO_x emissions. Overall, the inversion results for the NH_3 and, to a lesser extent, NO_x emissions are fairly robust with respect to the inverse modeling assumptions.

The uncertainty of the emissions after the inversion is estimated to decrease most strongly in locations where observational constraints are most significant (up to 50% reduction in uncertainty). The resulting emissions estimates show little correlation in space, though nearest neighbor emissions can be anti-correlated, and for a single emitted species, co-located emissions estimates from individual sectors are moderately anti-correlated. These anti-correlations are an indication that the amount of observations, in addition to the coarse model resolution, are not entirely sufficient to distinguish such sources. Hence, estimated redistributions within a sector are not entirely independent. Between species, emissions of NH_3 can become either correlated or anti-correlated with emissions of NO_x, depending upon the local environment, though such correlations were generally small.

Independent observations of NH_4^+ from CASTNet stations are used as an additional assessment of the optimized emissions. The comparison of the model NH_4^+ with the CASTNet observations generally shows a reduction in model bias after the inversion. The model still overestimates NH_4^+ in the Northeast by as much as $2\,\mu g/m^3$; however, changes to the NH_4^+ simulation incurred by assimilating observations of sulfate and nitrate are overall in the right direction throughout the year, and the model shows some improvement in the capturing the observed variance, particularly in July. Gilliland et al. (2006) concluded that observations of wet NH_4^+ (i.e., dissolved NH_3 and aerosol NH_4^+) are required to constrain NH_3 emissions unless the sulfate and nitrate budgets were verified. Similarly, Pinder et al. (2006) found that observations of aerosol NH_4^+ alone can not sufficiently constrain NH_3 emissions throughout much of the year. Here we have, in essence, taken the opposite approach by applying an inverse modeling tool explicitly capable of exploiting the dependancy between the inorganic $PM_{2.5}$ constituents, thus utilizing measurements of sulfate and nitrate to provide constraints on estimates of NH_3 emissions. A benefit of this approach is that sulfate and nitrate aerosol measurements may be more readily available then those of NH_x or precipitated ammonium.

Adjoint models can provide detailed insight into the influence of emissions on model estimates of air quality nonattainment of inorganic $PM_{2.5}$. Previous works have highlighted the fundamental difficulties in controlling inorganic $PM_{2.5}$ arising from the interactions of inorganic aerosol components (West et al., 1999; Vayenas et al., 2005) and for the importance of NH_3 controls, particularly in winter (Takahama et al., 2004; Pinder et al., 2007), and SO_x controls in summer (Pinder et al., 2007). The present work demonstrates how the effectiveness of emissions control strategies for emissions changes in all model locations and source sectors are readily addressed using sensitivities calculated with the adjoint model. An attainment metric is considered that represents the peak inorganic $PM_{2.5}$ concentrations that are of concern for NAAQS. The disparity between locations of peak emissions, regions of nonattainment and locations of the nonattainment sensitivities, highlights the importance of transport, chemistry and thermodynamics in the formation of this type of aerosol from gas-phase precursors, and the complications that thus arise when devising local control strategies for air quality attainment of secondary pollutants. Controls of NH_3 emissions are estimated to be most effective in locations where their emissions contribute to peak concentrations of inorganic $PM_{2.5}$. In July, October and January, this is near sources of SO_x rather than peak NH_3 emissions. As such, this analysis shows that the emissions abatement at locations of the largest NH_3 emissions may in some seasons be inconsequential, particularly when compared to emissions abatement elsewhere. NO_x controls are estimated to be most effective in October, and even more effective than SO_x or NH_3 controls in northern areas. In January, it is estimated that conditions could be such that reduction of SO_x leads to increases in the $PM_{2.5}$ concentrations. NH_3 controls are estimated to be more effective in January and April, and SO_x controls more effective in July, consistent with the findings of Pinder et al. (2007).

Analysis of the total effectiveness of emissions from individual sectors, as compared to the distributions of the emissions themselves, indicates that certain emissions sectors are more effective targets for abatement. In particular, emissions of SO_x and NO_x from stack (industrial) sources are found to be more influential than the surface (transport) sector. Emissions of NH_3 from biofuel and natural sources are more influential than from anthropogenic sources. While these distinctions are dependent upon the spatial and temporal distributions of the emissions, in this case the emissions themselves have been constrained by observations, which is an advantage of the two-stage analysis of inorganic $PM_{2.5}$ sources taken in this present work over sensitivity analysis alone.

The utility of the adjoint model for analysis of long-range influences is also demonstrated. Intercontinental influence is found to be minimal for estimates of peak air quality exceedences; however, there is some influence in ambient concentrations. As noted in previous works by Park et al. (2004, 2006), such influence, while small, could have important consequences for attainment of regional haze goals; such levels may also be of concern for public health, regardless of NAAQS thresholds (Schwartz et al., 2002, 2008). Within North America, a substantial fraction (23.9%) of the influence by the surface SO_x emissions sector comes from Mexico, while 16.7% of the influence by the stack SO_x sector comes from Canada. Other sectors have large percent influences from outside the US (e.g., biofuel) but have small overall impact. Further inverse modeling using observations outside the US is necessary to constrain the magnitude of distant emissions, which is evidently warranted.

Comprehensive analysis of sources of inorganic $PM_{2.5}$ using an adjoint model is demonstrated to be a powerful new framework for assessing emissions abatement strategies aimed at $PM_{2.5}$ air quality attainment. This method is advantageous owing to the efficiency at which influences from all source types and locations are revealed, and because such sensitivities are calculated with respect to the current observationally constrained estimates of the magnitudes of the aerosol sources. An additional benefit is that the adjoint model affords simultaneous analysis of additional model parameters, such as chemical reaction rates and initial conditions. This approach is shown to provide important insight into the variability of the influence of emissions in different locations, seasons, and from different sectors. In contrast to alternative approaches to source analysis (emissions labeling or toggling), the adjoint model results are not source attributions. However, interpretation of the adjoint sensitivities as the effectiveness of incremental changes to existing emissions for attaining air quality standards is shown to be of particular value for decision making activities focusing on emissions mitigation strategies.

Acknowledgements. This work was supported by US Environmental Protection Agency, grant R832158, a Columbia University Earth Institute Postdoctoral Fellowship, and NASA's Atmospheric Chemistry Modeling and Analysis Program. Thanks are also given to supercomputing resources at NCCS and JPL.

Edited by: A. Nenes

References

Adams, P. J., Seinfeld, J. H., and Koch, D. M.: Global concentrations of tropospheric sulfate, nitrate, and ammonium aerosol simulated in a general circulation model, J. Geophys. Res.-Atmos., 104, 13791–13823, 1999.

Alexander, B., Park, R. J., Jacob, D. J., Li, Q. B., Yantosca, R. M., Savarino, J., Lee, C. C. W., and Thiemens, M. H.: Sulfate formation in sea-salt aerosols: Constraints from oxygen isotopes, J. Geophys. Res.-Atmos., 110, D10307, doi:10.1029/2004JD005659, 2005.

Baumgardner, R. E., Lavery, T. F., Rogers, C. M., and Isil, S. S.: Estimates of the atmospheric deposition of sulfur and nitrogen species: Clean Air Status and Trends Network, 1990–2000, Environ. Sci. Technol., 36, 2614–2629, 2002.

Beer, R., Shephard, M. W., Kulawik, S., Clough, S. A., Eldred, R. A., Bowman, K. W., Sander, S. P., Fisher, B. M., Payne, V. H., Louo, M., Osterman, G. B., and Worden, J. R.: First satellite observations of lower tropospheric ammonia and methanol, Geophys. Res. Lett., 35, L09801, doi:10.1029/2008GL033642, 2008.

Benkovitz, C. M., Scholtz, M. T., Pacyna, J., Tarrason, L., Dignon, J., Voldner, E. C., Spiro, P. A., Logan, J. A., and Graedel, T. E.: Global gridded inventories of anthropogenic emissions of sulfur and nitrogen, J. Geophys. Res.-Atmos., 101, 29239–29253, 1996.

Benkovitz, C. M., Schwartz, S. E., Jensen, M. P., and Miller, M. A.: Attribution of modeled atmospheric sulfate and SO2 in the Northern Hemisphere for JuneJuly 1997, Atmos. Chem. Phys., 6, 4723–4738, 2006, http://www.atmos-chem-phys.net/6/4723/2006/.

Bey, I., Jacob, D. J., Yantosca, R. M., Logan, J. A., Field, B. D., Fiore, A. M., Li, Q. B., Liu, H. G. Y., Mickley, L. J., and Schultz, M. G.: Global modeling of tropospheric chemistry with assimilated meteorology: Model description and evaluation, J. Geophys. Res.-Atmos., 106, 23073–23095, 2001.

Binkowski, F. S. and Roselle, S. J.: Models-3 community multiscale air quality (CMAQ) model aerosol component – 1. Model description, J. Geophys. Res.-Atmos., 108, 4183, doi:10.1029/2001JD001409, 2003.

Bouwman, A. F., Lee, D. S., Asman, W. A. H., Dentener, F. J., VanderHoek, K. W., and Olivier, J. G. J.: A global high-resolution emission inventory for ammonia, Global Biogeochem. Cycles, 11, 561–587, 1997.

Brinkman, G., Vance, G., Hannigan, M. P., and Milford, J. B.: Use of synthetic data to evaluate positive matrix factorization as a source apportionment tool for $PM_{2.5}$ exposure data, Environ. Sci. Technol., 40, 1892–1901, 2006.

Brock, C. A., Sullivan, A. P., Peltier, R. E., Weber, R. J., Wollny, A., de Gouw, J. A., Middlebrook, A. M., Atlas, E. L., Stohl, A., Trainer, M. K., Cooper, O. R., Fehsenfeld, F. C., Frost, G. J., Holloway, J., Hübler, G., Neuman, J. A., Ryerson, T. B., Warneke, C., and Wilson, J. C.: Sources of particulate matter in the northeastern United States in summer: 2. Evolution of chem-

ical and microphysical properties, J. Geophys. Res.-Atmos., 113, D08302, doi:10.1029/2007JD009241, 2008.

Brown, S. S., Ryerson, T. B., Wollny, A. G., Brock, C. A., Peltier, R., Sullivan, A. P., Weber, R. J., Dube, W. P., Trainer, M., Meagher, J. F., Fehsenfeld, F. C., and Ravishankara, A. R.: Variability in nocturnal nitrogen oxide processing and its role in regional air quality, Science, 311, 67–70, 2006.

Byrd, R. H., Lu, P. H., Nocedal, J., and Zhu, C. Y.: A Limited Memory Algorithm for Bound Constrained Optimization, Siam J. Sci. Comput., 16, 1190–1208, 1995.

Chai, T. F., Carmichael, G. R., Sandu, A., Tang, Y. H., and Daescu, D. N.: Chemical data assimilation of Transport and Chemical Evolution over the Pacific (TRACE-P) aircraft measurements, J. Geophys. Res.-Atmos., 111, D02301, doi:10.1029/2005JD005883, 2006.

Chai, T. F., Carmichael, G. R., Tang, Y. H., Sandu, A., Hardesty, M., Pilewskie, P., Whitlow, S., Browell, E. V., Avery, M. A., Nedelec, P., Merrill, J. T., Thompson, A. M., and Williams, E.: Four-dimensional data assimilation experiments with International Consortium for Atmospheric Research on Transport and Transformation ozone measurements, J. Geophys. Res.-Atmos., 112, D12S15, doi:10.1029/2006jd007763, 2007.

Chin, M., Rood, R. B., Lin, S. J., Muller, J. F., and Thompson, A. M.: Atmospheric sulfur cycle simulated in the global model GOCART: Model description and global properties, J. Geophys. Res.-Atmos., 105, 24671–24687, 2000.

Chin, Mian, Diehl, T., Ginoux, P., and Malm, W.: Intercontinental transport of pollution and dust aerosols: implications for regional air quality, Atmos. Chem. Phys., 7, 5501–5517, 2007, http://www.atmos-chem-phys.net/7/5501/2007/.

de Gouw, J. A., Brock, C. A., Atlas, E. L., Bates, T. S., Fehsenfeld, F. C., Goldan, P. D., Holloway, J. S., Kuster, W. C., Lerner, B. M., Matthew, B. M., Middlebrook, A. M., Onasch, T. B., Peltier, R. E., Quinn, P. K., Senff, C. J., Stohl, A., Sullivan, A. P., Trainer, M., Warneke, C., Weber, R. J., and Williams, E. J.: Sources of particulate matter in the northeastern United States in summer: 1. Direct emissions and secondary formation of organic matter in urban plumes, J. Geophys. Res.-Atmos., 113, D08301, doi:10.1029/2007jd009243, 2008.

Dentener, F. J. and Crutzen, P. J.: Reaction of N_2O_5 on tropospheric aerosols - Impact on the global distributions of NO_x, O_3, and OH, J. Geophys. Res.-Atmos., 98, 7149–7163, 1993.

Dubovik, O., Lapyonok, T., Kaufman, Y. J., Chin, M., Ginoux, P., Remer, L. A., and Holben, B. N.: Inversion of global distribution of aerosol sources using MODIS and AERONET data, Optica Pura y Aplicada, 37, 3349–3358, 2004.

Dubovik, O., Lapyonok, T., Kaufman, Y. J., Chin, M., Ginoux, P., Kahn, R. A., and Sinyuk, A.: Retrieving global aerosol sources from satellites using inverse modeling, Atmos. Chem. Phys., 8, 209–250, 2008, http://www.atmos-chem-phys.net/8/209/2008/.

Duncan, B. N., Martin, R. V., Staudt, A. C., Yevich, R., and Logan, J. A.: Interannual and seasonal variability of biomass burning emissions constrained by satellite observations, J. Geophys. Res.-Atmos., 108(D2), 4100, doi:10.1029/2002JD002378, 2003.

Elbern, H., Schmidt, H., and Ebel, A.: Variational data assimilation for tropospheric chemistry modeling, J. Geophys. Res.-Atmos., 102, 15967–15985, 1997.

Elbern, H., Schmidt, H., Talagrand, O., and Ebel, A.: 4D-varational data assimilation with an adjoint air quality model for emission analysis, Environ. Modell. Softw., 15, 539–548, 2000.

Environmental Protection Agency (EPA): Latest findings on national air quality: 2001 status and trends, Tech. rep., 2002.

Environmental Protection Agency (EPA), TTN NAAQS – $PM_{2.5}$ – NAAQS Implementation $PM_{2.5}$ Designations – Technical Information, 2004.

Evans, M. J. and Jacob, D. J.: Impact of new laboratory studies of N_2O_5 hydrolysis on global model budgets of tropospheric nitrogen oxides, ozone, and OH, Geophys. Res. Lett., 32, L09813, doi:10.1029/2005GL022469, 2005.

Fairlie, T. D., Jacob, D. J., and Park, R. J.: The impact of transpacific transport of mineral dust in the United States, Atmos. Environ., 41, 1251–1266, 2007.

Fisher, M. and Lary, D. J.: Lagrangian four-dimensional variational data assimilation of chemical species, Q. J. R. Meteorol. Soc., 121, 1681–1704, 1995.

Fountoukis, C., Nenes, A., Sullivan, A., Weber, R., Van Reken, T., Fischer, M., Matas, E., Moya, M., Farmer, D., and Cohen, R. C.: Thermodynamic characterization of Mexico City aerosol during MILAGRO 2006, Atmos. Chem. Phys., 9, 2141–2156, 2009, http://www.atmos-chem-phys.net/9/2141/2009/.

Giering, R. and Kaminski, T.: Recipes for adjoint code construction, ACM Transactions on Mathematical Software, 24, 437–474, 1998.

Gilliland, A. and Abbitt, P. J.: A sensitivity study of the discrete Kalman filter (DKF) to initial condition discrepancies, J. Geophys. Res.-Atmos., 106, 17939–17952, 2001.

Gilliland, A. B., Dennis, R. L., Roselle, S. J., and Pierce, T. E.: Seasonal NH_3 emission estimates for the eastern United States based on ammonium wet concentrations and an inverse modeling method, J. Geophys. Res.-Atmos., 108, 4477, doi:10.1029/2002JD003063, 2003.

Gilliland, A. B., Appel, K. W., Pinder, R. W., and Dennis, R. L.: Seasonal NH_3 emissions for the continental United States: Inverse model estimation and evaluation, Atmos. Environ., 40, 4986–4998, 2006.

Hakami, A., Henze, D. K., Seinfeld, J. H., Chai, T., Tang, Y., Carmichael, G. R., and Sandu, A.: Adjoint inverse modeling of black carbon during the Asian Pacific Regional Aerosol Characterization Experiment, J. Geophys. Res.-Atmos., 110, D14301, doi:10.1029/2004JD005671, 2005.

Hakami, A., Seinfeld, J. H., Chai, T. F., Tang, Y. H., Carmichael, G. R., and Sandu, A.: Adjoint sensitivity analysis of ozone nonattainment over the continental United States, Environ. Sci. Technol., 40, 3855–3864, 2006.

Hakami, A., Henze, D. K., Seinfeld, J. H., Singh, K., Sandu, A., Kim, S., Byun, D., and Li, Q.: The adjoint of CMAQ, Environ. Sci. Technol., 41, 7807–7817, 2007.

Hansen, P. C.: Rank-Deficient and Discrete Ill-Posed Problems: Numerical Aspects of Linear Inversion, SIAM, Philadelphia, USA, 1998.

Heald, C. L., Jacob, D. J., Park, R. J., Russell, L. M., Huebert, B. J., Seinfeld, J. H., Liao, H., and Weber, R. J.: A large organic aerosol source in the free troposphere missing from current models, Geophys. Res. Lett., 32, L18809, doi:10.1029/2005GL023831, 2005.

Heald, C. L., Jacob, D. J., Park, R. J., Alexander, B., Fairlie, T. D., Chu, D. A., and Yantosca, R. M.: Transpacific transport of Asian anthropogenic aerosols and its impact on surface air quality in

the United States, J. Geophys. Res.-Atmos., 111, D14310, doi:doi:10.1029/2005JD006847, 2006a.

Heald, C. L., Jacob, D. J., Turquety, S., Hudman, R. C., Weber, R. J., Sullivan, A. P., Peltier, R. E., Atlas, E. L., de Gouw, J. A., Warneke, C., Holloway, J. S., Neuman, J. A., Flocke, F. M., and Seinfeld, J. H.: Concentrations and sources of organic carbon aerosols in the free troposphere over North America, J. Geophys. Res.-Atmos., 111, D23S47, doi:10.1029/2006JD007705, 2006b.

Hennigan, C. J., Sullivan, A. P., Fountoukis, C. I., Nenes, A., Hecobian, A., Vargas, O., Peltier, R. E., Case Hanks, A. T., Huey, L. G., Lefer, B. L., Russell, A. G., and Weber, R. J.: On the volatility and production mechanisms of newly formed nitrate and water soluble organic aerosol in Mexico City, Atmos. Chem. Phys., 8, 3761–3768, 2008, http://www.atmos-chem-phys.net/8/3761/2008/.

Hennigan, C. J., Bergin, M. H., Russell, A. G., Nenes, A., and Weber, R. J.: Gas/particle partitioning of water-soluble organic aerosol in Atlanta, Atmos. Chem. Phys., 9, 3613–3628, 2009, http://www.atmos-chem-phys.net/9/3613/2009/.

Henze, D. K., Seinfeld, J. H., Liao, W., Sandu, A., and Carmichael, G. R.: Inverse modeling of aerosol dynamics: Condensational growth, J. Geophys. Res.-Atmos., 109, D14201, doi:10.1029/2004JD004593, 2004.

Henze, D. K., Hakami, A., and Seinfeld, J. H.: Development of the adjoint of GEOS-Chem, Atmos. Chem. Phys., 7, 2413–2433, 2007, http://www.atmos-chem-phys.net/7/2413/2007/.

Jacob, D. J., Liu, H., Mari, C., and Yantosca, B. M.: Harvard wet deposition scheme for GMI, http://gmi.gsfc.nasa.gov/models/jacob_wetdep.pdf, 2000.

Jaffe, D., McKendry, I., Anderson, T., and Price, H.: Six "new" episodes of trans-Pacific transport of air pollutants, Atmos. Environ., 37, 391–404, doi:PiiS1352-2310(02)00862-2, 2003.

Kalnay, E.: Atmospheric Modeling, Data Assimilation and Predictability, Cambridge University Press, Cambridge, United Kingdom, 2003.

Kim, S. W., Heckel, A., McKeen, S. A., Frost, G. J., Hsie, E. Y., Trainer, M. K., Richter, A., Burrows, J. P., Peckham, S. E., and Grell, G. A.: Satellite-observed US power plant NOx emission reductions and their impact on air quality, Geophys. Res. Lett., 33, L22812, doi:10.1029/2006gl027749, 2006.

Kleeman, M. J. and Cass, G. R.: A 3D Eulerian source-oriented model for an externally mixed aerosol, Environ. Sci. Technol., 35, 4834–4848, 2001.

Knipping, E. M., Kumar, N., Pun, B. K., Seigneur, C., Wu, S. Y., and Schichtel, B. A.: Modeling regional haze during the BRAVO study using CMAQ-MADRID: 2. Source region attribution of particulate sulfate compounds, J. Geophys. Res.-Atmos., 111, D06303, doi:10.1029/2004JD005609, 2006.

Koo, B., Dunker, A. M., and Yarwood, G.: Implementing the decoupled direct method for sensitivity analysis in a particulate matter air quality model, Environ. Sci. Technol., 41, 2847–2854, 2007.

Kopacz, M., Jacob, D., Henze, D. K., Heald, C. L., Streets, D. G., and Zhang, Q.: A comparison of analytical and adjoint Bayesian inversion methods for constraining Asian sources of CO using satellite (MOPITT) measurements of CO columns, J. Geophys. Res.-Atmos., 114, D04305, doi:10.1029/2007JD009264, 2009.

Lee, S., Liu, W., Wang, Y., Russell, A. G., and Edgerton, E. S.: Source apportionment of $PM_{2.5}$: Comparing PMF and CMB results for four ambient monitoring sites in the southeastern United States, Atmos. Environ., 42, 4126–4137, 2008.

Li, Q. B., Jacob, D. J., Logan, J. A., Bey, I., Yantosca, R. M., Liu, H. Y., Martin, R. V., Fiore, A. M., Field, B. D., Duncan, B. N., and Thouret, V.: A tropospheric ozone maximum over the Middle East, Geophys. Res. Lett., 28, 3235–3238, 2001.

Liao, H., Henze, D. K., Seinfeld, J. H., Wu, S., and Mickley, L. J.: Biogenic secondary organic aerosol over the United States: Comparison of climatological simulations with observations, J. Geophys. Res.-Atmos., 112, D06201, doi:10.1029/2006JD007813, 2007.

Lions, J. L.: Optimal Control of Systems Governed by Partial Differential Equations, Springer-Verlag, Berlin, 1971.

Liu, J., Mauzerall, D. L., and Horowitz, L. W.: Source-receptor relationships between East Asian sulfur dioxide emissions and Northern Hemisphere sulfate concentrations, Atmos. Chem. Phys., 8, 3721–3733, 2008, http://www.atmos-chem-phys.net/8/3721/2008/.

Malm, W. C., Schichtel, B. A., Pitchford, M. L., Ashbaugh, L. L., and Eldred, R. A.: Spatial and monthly trends in speciated fine particle concentration in the United States, J. Geophys. Res.-Atmos., 109, D03306, 10.1029/2003jd003739, 2004.

Malm, W. C., Sisler, J. F., Huffman, D., Eldred, R. A., and Cahill, T. A.: Spatial and seasonal trends in particle concentration and optical extinction in the United States, J. Geophys. Res.-Atmos., 99, 1347–1370, 1994.

Marchuk, G.: Numerical solution of the problems of the dynamics of the atmosphere and the ocean (In Russian), Gidrometeoizdat, 1974.

Martien, P. T. and Harley, R. A.: Adjoint sensitivity analysis for a three-dimensional photochemical model: Application to Southern California, Environ. Sci. Technol., 40, 4200–4210, 2006.

Martien, P. T., Harley, R. A., and Cacuci, D. G.: Adjoint sensitivity analysis for a three-dimensional photochemical model: Implementation and method comparison, Environ. Sci. Technol., 40, 2663–2670, 2006.

Martin, R. V., Jacob, D. J., Logan, J. A., Bey, I., Yantosca, R. M., Staudt, A. C., Li, Q. B., Fiore, A. M., Duncan, B. N., Liu, H. Y., Ginoux, P., and Thouret, V.: Interpretation of TOMS observations of tropical tropospheric ozone with a global model and in situ observations, J. Geophys. Res.-Atmos., 107, 4351, doi:10.1029/2001JD001480, 2002.

Martin, R. V., Jacob, D. J., Yantosca, R. M., Chin, M., and Ginoux, P.: Global and regional decreases in tropospheric oxidants from photochemical effects of aerosols, J. Geophys. Res.-Atmos., 108, 4097, doi:10.1029/2002JD002622, 2003.

Mendoza-Dominguez, A. and Russell, A. G.: Iterative inverse modeling and direct sensitivity analysis of a photochemical air duality model, Environ. Sci. Technol., 34, 4974–4981, 2000.

Mendoza-Dominguez, A. and Russell, A. G.: Emission strength validation using four-dimensional data assimilation: Application to primary aerosol and precursors to ozone and secondary aerosol, J. Air & Waste Manage. Assoc, 51, 1538–1550, 2001.

Menut, L.: Adjoint modeling for atmospheric pollution process sensitivity at regional scale, J. Geophys. Res.-Atmos., 108, 8562, doi:10.1029/2002JD002549, 2003.

Müller, J.-F. and Stavrakou, T.: Inversion of CO and NO_x emissions using the adjoint of the IMAGES model, Atmos. Chem. Phys., 5, 1157–1186, 2005, http://www.atmos-chem-phys.net/5/1157/2005/.

Napelenok, S. L., Cohan, D., Hu, Y., and Russel, A. G.: Decoupled direct 3D sensitivity analysis for particulate matter (DDM-3DPM), Atmos. Environ., 40, 6112–6121, 2006.

Nester, K. and Panitz, H.-J.: Sensitivity analysis by the adjoint chemistry transport model DRAISfor an episode in the Berlin Ozone (BERLIOZ) experiment, Atmos. Chem. Phys., 6, 2091–2106, 2006, http://www.atmos-chem-phys.net/6/2091/2006/.

Nowak, J. B., Huey, L. G., Russell, A. G., Tian, D., Neuman, J. A., Orsini, D., Sjostedt, S. J., Sullivan, A. P., Tanner, D. J., Weber, R. J., Nenes, A., Edgerton, E., and Fehsenfeld, F. C.: Analysis of urban gas phase ammonia measurements from the 2002 Atlanta Aerosol Nucleation and Real-Time Characterization Experiment (ANARChE), J. Geophys. Res.-Atmos., 111, D17308, doi:10.1029/2006JD007113, 2006.

Park, R. J., Jacob, D., Field, B. D., Yantosca, R., and Chin, M.: Natural and transboundary pollution influences on sulfate-nitrate-ammonium aerosols in the United States: Implications for policy, J. Geophys. Res.-Atmos., 109, D15204, doi:10.1029/2003JD004473, 2004.

Park, R. J., Jacob, D. J., Kumar, N., and Yantosca, R. M.: Regional visibility statistics in the United States: Natural and transboundary pollution influences, and implications for the Regional Haze Rule, Atmos. Environ., 40, 5405–5423, 2006.

Pinder, R. W., Adams, P. J., Pandis, S. N., and Gilliland, A. B.: Temporally resolved ammonia emission inventories: Current estimates, evaluation tools, and measurement needs, J. Geophys. Res.-Atmos., 111, D16310, doi:10.1029/2005JD006603, 2006.

Pinder, R. W., Adams, P. J., and Pandis, S. N.: Ammonia emission controls as a cost-effective strategy for reducing atmospheric particulate matter in the eastern United States, Environ. Sci. Technol., 41, 380–386, 2007.

Pope, C. A.: Review: Epidemiological basis for particulate air pollution health standards, Aerosol Sci. Tech., 32, 4–14, 2000.

Pope, C. A., Burnett, R. T., Thun, M. J., Calle, E. E., Krewski, D., Ito, K., and Thurston, G. D.: Lung cancer, cardiopulmonary mortality, and long-term exposure to fine particulate air pollution, J. Am. Med. Assoc., 287, 1132–1141, 2002.

Quelo, D., Mallet, V., and Sportisse, B.: Inverse modeling of NO_x emissions at regional scale over northern France: Preliminary investigation of the second-order sensitivity, J. Geophys. Res.-Atmos., 110, D24310, doi:10.1029/2005JD006151, 2005.

Quinn, P. K., Bates, T. S., Coffman, D., Onasch, T. B., Worsnop, D., Baynard, T., de Gouw, J. A., Goldan, P. D., Kuster, W. C., Williams, E., Roberts, J. M., Lerner, B., Stohl, A., Pettersson, A., and Lovejoy, E. R.: Impacts of sources and aging on submicrometer aerosol properties in the marine boundary layer across the Gulf of Maine, J. Geophys. Res.-Atmos., 111, D23S36, doi:10.1029/2006jd007582, 2006.

Reiss, R., Anderson, E. L., Cross, C. E., Hidy, G., Hoel, D., McClellan, R., and Moolgavkar, S.: Evidence of health impacts of sulfate- and nitrate-containing particles in ambient air, Inhal Toxicol, 19, 419–449, doi:10.1080/08958370601174941, 2007.

Rodgers, C. D.: Inverse Methods for Atmospheric Sounding, vol. 2 of Series on Atmospheric, Oceanic and Planetary Physics, World Scientific, Singapore, 2000.

Sandu, A., Daescu, D. N., Carmichael, G. R., and Chai, T. F.: Adjoint sensitivity analysis of regional air quality models, J. Comput. Phys., 204, 222–252, 2005a.

Sandu, A., Liao, W., Carmichael, G. R., Henze, D. K., and Seinfeld, J. H.: Inverse modeling of aerosol dynamics using adjoints: Theoretical and numerical considerations, Aerosol Sci. Tech., 39, 677–694, 2005b.

Schmidt, H. and Martin, D.: Adjoint sensitivity of episodic ozone in the Paris area to emissions on the continental scale, J. Geophys. Res.-Atmos., 108, 8561, doi:10.1029/2001JD001583, 2003.

Schwartz, J., Laden, F., and Zanobetti, A.: The concentration-response relation between $PM_{2.5}$ and daily deaths, Environ. Health Perspect., 110, 1025–1029, 2002.

Schwartz, J., Coull, B., Laden, F., and Ryan, L.: The effect of dose and timing of dose on the association between airborne particles and survival, Environ. Health Perspect., 116, 64–69, doi:Doi10.1289/Ehp.9955, 2008.

Stavrakou, T. and Muller, J. F.: Grid-based versus big region approach for inverting CO emissions using Measurement of Pollution in the Troposphere (MOPITT) data, J. Geophys. Res.-Atmos., 111, D15304, doi:10.1029/2005JD006896, 2006.

Stavrakou, T., Müller, J.-F., Boersma, K. F., Smedt, I. D., and van der A., R. J.: Assessing the distribution and growth rates of NO_x emission sources by inverting a 10-year record of NO_2 satellite columns, Geophys. Res. Lett., 35, L10801, doi:10.1029/2008GL033521, 2008.

Stephen, K. and Aneja, V. P.: Trends in agricultural ammonia emissions and ammonium concentrations in precipitation over the Southeast and Midwest United States, Atmos. Environ., 42, 3238–3252, 2008.

Stier, P., Seinfeld, J. H., Kinne, S., Feichter, J., and Boucher, O.: Impact of nonabsorbing anthropogenic aerosols on clear-sky atmospheric absorption, J. Geophys. Res.-Atmos., 111, D18201, doi:10.1029/2006jd007147, 2006.

Surratt, J. D., Kroll, J. H., Kleindienst, T. E., Edney, E. O., Claeys, M., Sorooshian, A., Ng, N. L., Offenberg, J. H., Lewandowski, M., Jaoui, M., Flagan, R. C., and Seinfeld, J. H.: Evidence for organosulfates in secondary organic aerosol, Environ. Sci. Technol., 41, 517–527, 2007.

Takahama, S., Wittig, A. E., Vayenas, D. V., Davidson, C. I., and Pandis, S. N.: Modeling the diurnal variation of nitrate during the Pittsburgh Air Quality Study, J. Geophys. Res.-Atmos., 109, D16S06, doi:10.1029/2003JD004149, 2004.

Tarantola, A.: Inverse problem theory and model parameter estimation, SIAM, 2005.

Tarantola, A.: Popper, Bayes and the inverse problem, Nat. Phys., 2, 492–494, 2006.

Thacker, W. C.: The role of the Hessian matrix in fitting models to measurements, J. Geophys. Res.-Oceans, 94, 6177–6196, 1989.

Thornton, J. and Abbatt, J. P. D.: Measurements of HO_2 uptake to aqueous aerosol: Mass accomodation coefficients and net reactive loss, J. Geophys. Res.-Atmos., 110, D08309, doi:10.1029/2004JD005402, 2005.

Tziperman, E. and Thacker, W. C.: An optimal-control/adjoint-equations approach to studying the oceanic general circulation, J. Phys. Oceonogr., 19, 1471–1485, 1989.

van der A., R. J., Eskes, H. J., Boersma, K. F., van Noije, T. P. C., Roozendael, M. V., Smedt, I. D., Peters, D. H. M. U., and Meijer, E. W.: Trends, seasonal variability and dominant NO_x source derived from a ten year record of NO_2 measured from space, J. Geophys. Res.-Atmos., 113, D04302, doi:10.1029/2007JD009021, 2008.

Vautard, R., Beekmann, M., and Menut, L.: Applications of ad-

joint modelling in atmospheric chemistry: Sensitivity and inverse modelling, Environ. Modell. Softw., 15, 703–709, 2000.

Vayenas, D. V., Takahama, S., Davidson, C. I., and Pandis, S. N.: Simulation of the thermodynamics and removal processes in the sulfate-ammonia-nitric acid system during winter: Implications for $PM_{2.5}$ control strategies, J. Geophys. Res.-Atmos., 110, D07S14, doi:10.1029/2004JD005038., 2005.

Volkamer, R., Ziemann, P. J., and Molina, M. J.: Secondary Organic Aerosol Formation from Acetylene (C_2H_2): seed effect on SOA yields due to organic photochemistry in the aerosol aqueous phase, Atmos. Chem. Phys., 9, 1907–1928, 2009, http://www.atmos-chem-phys.net/9/1907/2009/.

Wang, Y. H., Jacob, D. J., and Logan, J. A.: Global simulation of tropospheric O_3-NO_x-hydrocarbon chemistry 1. Model formulation, J. Geophys. Res.-Atmos., 103, 10713–10725, 1998.

Wesely, M. L.: Parameterization of surface resistances to gaseous dry deposition in regional-scale numerical-models, Atmos. Environ., 23, 1293–1304, 1989.

West, J. J., Ansari, A. S., and Pandis, S. N.: Marginal $PM_{2.5}$: Nonlinear aerosol mass response to sulfate reductions in the Eastern United States, J. Air Waste Manage. Assoc., 49, 1415–1424, 1999.

Wu, S.-Y., Hu, J.-L., Zhang, Y., and Aneja, V. P.: Modeling atmospheric transport and fate of ammonia in North Carolina–Part II: Effect of ammonia emissions on fine particulate matter formation, Atmos. Environ., 42, 3437–3451, 2008.

Yevich, R. and Logan, J. A.: An assessment of biofuel use and burning of agricultural waste in the developing world, Global Biogeochem. Cycles, 17(4), 1095, doi:10.1029/2002GB001952, 2003.

Yienger, J., Galanter, M., Holloway, J., Phadnis, M., Guttikunda, S. K., Carmichael, G. R., Moxim, W. J., and Levy, H. I.: The episodic nature of air pollution transport from Asia to North America, J. Geophys. Res.-Atmos., 105, 26931–26945, 2000.

Ying, Q. and Kleeman, M. J.: Source contributions to the regional distribution of secondary particulate matter in California, Atmos. Environ., 40, 736–752, 2006.

Ying, Q., Fraser, M. P., Griffin, R. J., Chen, J. J., and Kleeman, M. J.: Verification of a source-oriented externally mixed air quality model during a severe photochemical smog episode, Atmos. Environ., 41, 1521–1538, 2007.

Yu, S., Eder, B., Dennis, R., Chu, S.-H., and Schwartz, S.: New unbiased symmetric metrics for the evaluation of air quality models, Atmos. Sci. Lett., 7, 26–34, doi:10.1002/asl.125, 2006.

Yu, S., Mathur, R., Schere, K., Kang, D., Pleim, J., Young, J., Tong, D., Pouliot, G., McKeen, S. A., and Rao, S. T.: Evaluation of real-time $PM_{2.5}$ forecasts and process analysis for $PM_{2.5}$ formation over the eastern United States using the Eta-CMAQ forecast model during the 2004 ICARTT study, J. Geophys. Res.-Atmos., 113, D06204, doi:10.1029/2007JD009226, 2008.

Yu, S. C., Dennis, R., Roselle, S., Nenes, A., Walker, J., Eder, B., Schere, K., Swall, J., and Robarge, W.: An assessment of the ability of three-dimensional air quality models with current thermodynamic equilibrium models to predict aerosol NO3-, J. Geophys. Res.-Atmos., 110, D07S13, doi:10.1029/2004jd004718, 2005.

Zhang, Y., Wu, S.-Y., Krishnan, S., Wang, K., Queen, A., Aneja, V. P., and Arya, S. P.: Modeling agricultural air quality: Current status, major challenges, and outlook, Atmos. Environ., 42, 3218–3237, 2008.

Zhu, C., Byrd, R. H., Lu, P., and Nocedal, J.: L-BFGS-B: A limited memory FORTRAN code for solving bound constrained optimization problems, Tech. rep., Northwestern University, 1994.